COLLEGE OF ENGINEERING
DEPARTMENT OF CIVIL ENGINEERING (CVEG)
STEEL STRUCTURES RESEARCH LABORATORY (SSRL)

SSRL Report N° 2016/1

Development of Pre-Stressed CFRP Fatigue Retrofits for Common Steel Bridge Connections

Korey Pough
Gary S. Prinz, Ph.D., P.E.

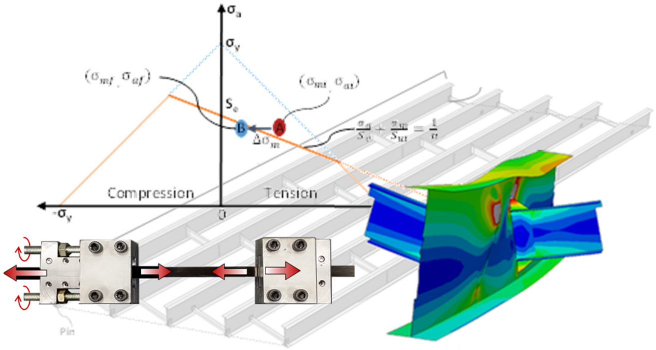

SSRL Project N° 0402-82227-21-5103
Final report submitted to the Southern Plains Transportation Center (SPTC)

July, 2016

COLLEGE OF ENGINEERING
DEPARTMENT OF CIVIL ENGINEERING (CVEG)
STEEL STRUCTURES RESEARCH LABORATORY (SSRL)

University of Arkansas
Department of Civil Engineering
4190 Bell Engineering Center
Fayetteville, AR 72701

Telephone : + 1 (479) 575-2494
Fax : + 1 (479) 575-7168
E-mail : prinz@uark.edu
Website : www.ssrl-uark.com

V/ref : **Fayetteville, AR, July 2016**
N/ref : CVEG **Report SSRL Nº 2016/1**

Development of Pre-Stressed CFRP Fatigue Retrofits for Common Steel Bridge Connections

Mandate:	Southern Plains Transportation Center (SPTC)
Mandate Description:	Investigation into corrosion tolerant pre-stressed CFRP fatigue retrofits for efficient bridge repair.
Date of Mandate:	July 2016
Specimens:	N/A
Reception of the Specimens:	N/A
Project Dates:	August 1, 2014 – July 31, 2016
UA Project Lead:	G.S. Prinz
Collaborators:	Royce Floyd (University of Oklahoma)
Report Authors:	K. Pough, and G.S. Prinz
SSRL Director:	G.S. Prinz

Signatures :
UA Project Lead

Gary S. Prinz, PhD, PE

This report contains 60 pages (including 14 pages of front matter)

[Page Intentionally Left Blank]

ACKNOWLEDGEMENTS

This report presents the results of a research project sponsored the U.S. Department of Transportation under Grant Award Number DTRT13-G-UTC36. The research was conducted in the Steel Structures Research Laboratory (SSRL) at the University of Arkansas through the Southern Plains Transportation Center led by University of Oklahoma. Although many individuals contributed to the research findings presented herein, the authors accept full responsibility for the conclusions presented.

[Page Intentionally Left Blank]

TABLE OF CONTENTS

RESEARCH REPORT

[Page Intentionally Left Blank]

LIST OF FIGURES

LIST OF TABLES

[Page Intentionally Left Blank]

NOTATION

The following terms are used in the text of this report:

A = S-N curve constant dependent on fatigue detail category;
$AASHTO$ = American Association of State Highway Transportation Officials;
$ADTT_{SL}$ = single lane average daily truck traffic;
A_m = cross-sectional area of region affected by retrofit;
A_p = cross-sectional area of the CFRP material;
$CFRP$ = carbon fiber reinforced polymer;
D_i = damage from individual cycle;
e = eccentricity;
F_{pre} = pre-stress force;
I_m = moment of inertia of region affected by retrofit;
k_a = endurance limit surface condition modification factor;
k_b = endurance limit size modification factor;
k_c = endurance limit load modification factor;
k_d = endurance limit temperature modification factor;
k_e = endurance limit reliability modification factor;
k_f = endurance limit miscellaneous effects modification factor;
n = number of stress cycles per truck passage;
N = number of cycles to failure;
S_{ut} = ultimate tensile stress;
S_e = fatigue endurance limit;
S_e' = fatigue endurance limit resulting from rotating beam test;
t_w = girder web thickness;
ΔF = nominal live-load stress range from fatigue truck;
ΔF_n = nominal fatigue resistance;
ΔF_{TH} = constant amplitude fatigue threshold;
$\Delta\sigma$ = applied stress range;
σ_m = mean stress;
σ_a = stress amplitude;
σ_{max} = maximum stress;
σ_{min} = minimum stress;
σ_{pre} = required pre-stress;

[Page Intentionally Left Blank]

RESEARCH REPORT

1. Introduction

1.1. *Overview*

Many bridges within the United States are currently classified as either structurally deficient (due to deterioration) or functionally obsolete (due to inconsistencies between past and present code requirements). A structurally deficient status may describe a bridge that has corroded elements or contains a structural defect (such as a crack) that requires repair. A functionally obsolete status describes the nature of a bridge in today's society. This status may be given to a bridge that contains narrow shoulders or lane widths, inadequate clearance for oversize vehicles, or does not meet current load carrying requirements. Of the more than 607,000 total US bridges, approximately 30% are currently classified as either structurally deficient or functionally obsolete (NACE, 2012). The status of steel bridges found within region 6 (Arkansas, Oklahoma, Louisiana, New Mexico, and Texas) of the Federal Highway Administration (FHWA) is similar to this national trend. Figure 1-1(a) shows the count and percentage of highway steel bridges within region 6 that are currently classified as structurally deficient, functionally obsolete, or not deficient and Figure 1-1(b) provides a more detailed breakdown by FHWA Region 6 States. From Figure 1-1(b) the majority of steel bridges within Oklahoma classify as either structurally deficient or functionally obsolete (over 3500 of the total 17400 bridges). Arkansas has over 1000 steel bridges classified as either deficient or obsolete. Note that the data in Figure 1-1 were collected from the National Bridge Inventory (NBI) database (Svirsky, 2015), which archives U.S. bridge information provided by state agencies. All data available in the NBI database were collected from each state Department of Transportation (DOT) back in 2012, indicating that estimations of structurally deficient bridges may be non-conservative. Only highway bridges are considered in this research (pedestrian and railway bridges are not included in the compiled data).

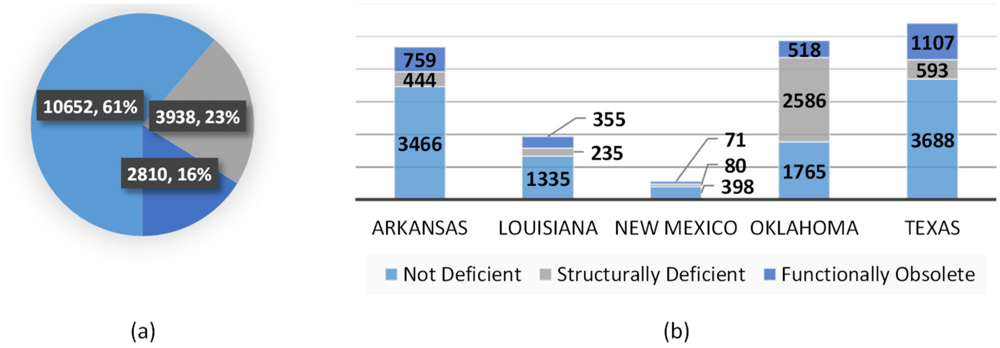

Figure 1-1: Status of Steel Highway Bridges in Region 6 (a) overall and (b) by state

Aging or deterioration of the nation's bridge infrastructure is a significant issue that requires attention. Causes for much of this deterioration can be attributed to two main factors, 1) corrosion, and 2) metallic fatigue, both of which work together to reduce the strength and serviceability of bridge components over time. As a result, many bridges are nearing or have reached their design fatigue lives, with cracks either existing or nearing initiation. In many cases, strengthening of the locally affected bridge components using localized retrofits is an economical and fast alternative to complete bridge replacement; however, such retrofits must be resilient to further corrosion and fatigue damage.

The objective of this research is to increase the longevity of existing steel bridges subjected to corrosion induced deterioration and metallic fatigue. This work will be accomplished by developing corrosion resistant retrofits using pre-stressed Carbon Fiber Reinforced Polymer (CFRP) materials to reinforce critical fatigue locations within steel components. CFRP is a promising retrofit material due to its strength to weight ratio, fatigue performance, and corrosion resistance.

This research is conducted in two parts. Figure 1-2 shows a flow chart of the research plan. In part 1 (Figure 1-2(a)), fatigue critical zones within common steel bridge components are identified and analyzed. Part 1 begins with an investigation of common bridges types within region 6 and a selection of four distinct bridges for analysis. Next, detailed finite element models simulating all bridge connection geometries are analyzed, considering the American Association of State Highway and Transportation Officials (AASHTO) Fatigue I Load Model. Finally, stress analyses are conducted and local stress ranges are characterized to determine the location of fatigue critical connection details within each bridge. In part 2 (Figure 1-2(b)), fatigue retrofits capable of extending the steel component fatigue life are developed using pre-stressed CFRP materials. Part 2 begins with the development of the retrofit configuration. Next, a fatigue evaluation is conducted on the critical fatigue detail in each bridge based on the Goodman fatigue criterion and the retrofit configuration. Finally, the retrofit is tested on a welded diaphragm to girder connection detail in a laboratory experiment.

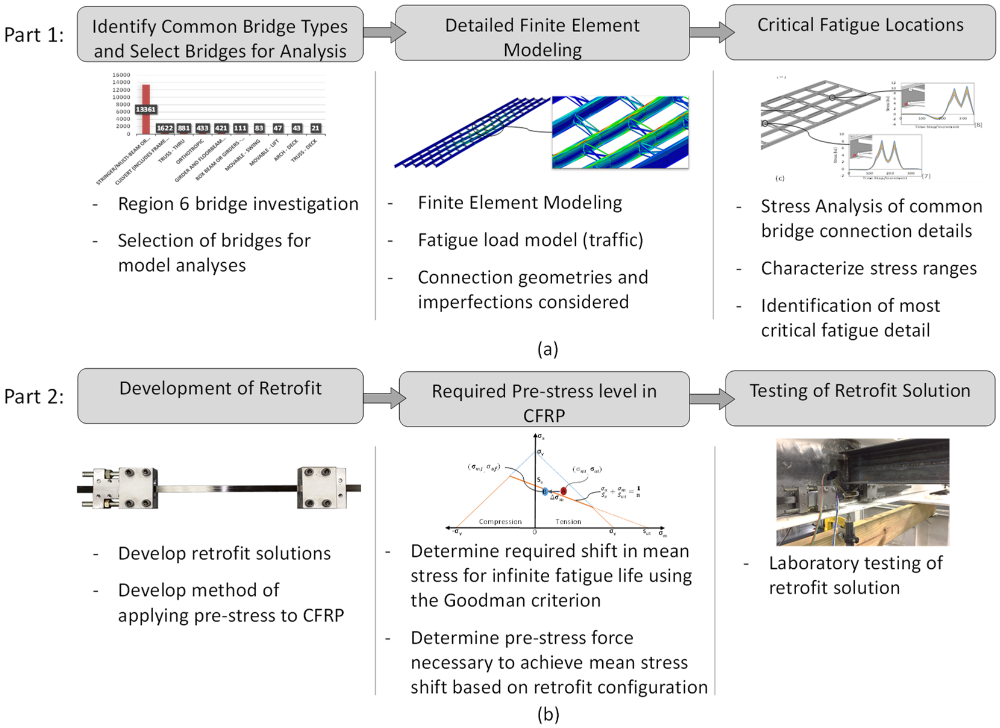

Figure 1-2: Description of Research Plan (a) Part 1: Identify fatigue critical zones. (b) Part 2: Develop retrofit solutions

2. Review of Relevant Literature

2.1. *Fatigue in Steel Bridges and Review of AASHTO Specification*

Fatigue is a phenomenon wherein a material is weakened due to repeated loading. The stresses that develop as a result of these repeated loads cause cracks that, as the repeated load conditions persist, can propagate to a critical size and cause structural failure. Bridges are common civil engineering structures that are prone to fatigue cracking. Fatigue is a significant concern, and component failure can result from applied stresses far below the static strength of the component materials.

Fatigue performance is controlled by the presence of pre-existing cracks or crack-like discontinuities, which often occur at welded connections or other areas of stress concentration (Mertz, 2012). As a result, the crack initiation phase often takes little or no time during the structure lifespan. While early steel bridges were constructed using built-up bolted or riveted connections, in the 1950's welding became a more popular bridge fabrication method due to ease of construction and its ability to create a rigid joint between elements. However, welding had two primary concerns regarding fatigue strength: 1) Welding introduces a more severe initial crack situation than bolting or riveting due to more critical stress concentrations and flaws (Mertz, 2012); and 2) The continuity between structural elements makes it possible for a crack in one element to propagate into an adjoining element (Mertz, 2012). Common bridge details that are susceptible to fatigue are identified in the specification for the design of steel bridges prepared by the American Association of State Highway and Transportation Officials (AASHTO) (AASHTO, 2012).

Common bridge components and details that are prone to fatigue cracking are grouped into eight categories called detail categories. Each detail category (A, B, B', C, C', D, E, and E') contains a unique fatigue tolerance based on the expected loading conditions. The AASHTO (2012) fatigue consideration specifies that each bridge detail must satisfy Equation 2-1:

$$\gamma(\Delta f) \leq (\Delta F)_n \qquad \text{Equation 2-1}$$

where γ is the fatigue load factor; (Δf) is the nominal live load stress range due to the passage of a fatigue truck; and $(\Delta F)_n$ is the nominal fatigue resistance. A fatigue load factor (γ) of 1.5 is used for Fatigue I load combinations (infinite fatigue life) while 0.75 is used for Fatigue II load combinations (finite fatigue life).

The nominal fatigue resistance $(\Delta F)_n$ is calculated based on the fatigue load combination for either infinite life (Equation 2-2) or finite life (Equation 2-3).

$$\text{Fatigue I:} \quad (\Delta F)_n = (\Delta F)_{TH} \qquad \text{Equation 2-2}$$

$$\text{Fatigue II:} \quad (\Delta F)_n = \left(\frac{A}{N}\right)^{\frac{1}{3}} \qquad \text{Equation 2-3}$$

$(\Delta F)_{TH}$ in Equation 2-2 is the constant amplitude fatigue threshold or fatigue limit. This value represents the allowable stress range for more than two million load cycles on a redundant load path structure. A bridge detail that experiences a stress range below this value will theoretically provide an infinite fatigue life. The constant A is specific to the detail category. Values for the constant A and $(\Delta F)_{TH}$ are given in Table 2-1 while N is the number of expected load cycles and is given by Equation 2-4.

Table 2-1: Constant A and $(\Delta F)_{TH}$ for AASHTO detail categories. (AASHTO 2012)

Detail Category	Constant A, times 108 (ksi3)	(ΔF)TH (ksi)
A	250.0	24.0
B	120.0	16.0
B’	61.0	12.0
C	44.0	10.0
C’	44.0	12.0
D	22.0	7.0
E	11.0	4.5
E’	3.9	2.6

$$N = (365)(75)n(ADTT)_{SL} \qquad \text{Equation 2-4}$$

In Equation 2-4, n is the number of stress cycles per truck passage; the value of n is given in the AASHTO specifications and is dependent upon span length and distance along the span. $(ADTT)_{SL}$ is the single-lane average daily truck traffic. Equation 2-3 is shown graphically in Figure 2-1 for each detail category.

The horizontal sections of the curves provided in Figure 2-1 represent the fatigue threshold $(\Delta F)_{TH}$. Values below this threshold represent a safe stress range for the corresponding number of cycles. The fatigue design life is considered to be 75 years in the overall development of the AASHTO 2012 specifications.

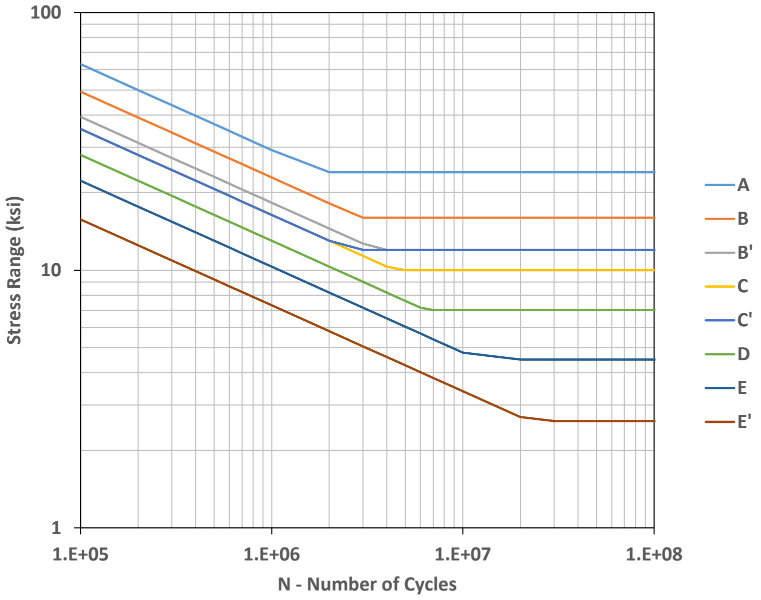

Figure 2-1: S-N Curves for each detail category

Although the current AASHTO code calls for a 75 year fatigue design life, this number has been lower in past specifications. The bridge service life was increased from 50 years to 75 years in the 1998 AASHTO specification (AASHTO, 1998). As a result, many steel bridges in the U.S. are approaching their original design life and will need to be examined and maintained to extend their service life. Additionally, many of these bridges may be classified as functionally obsolete if its original design does not meet the current specification requirement. Figure 2-2 shows the distribution of steel highway bridges by age in region 6.

The data provided in Figure 2-2 were collected up to 2013. From Figure 2-2, nearly 70 percent of bridges within FHWA Region 6 were designed for a 50 year fatigue design life (assuming that all bridges constructed before 1998, 15 years old as of 2013, were designed for 50 years). Additionally from Figure 2-2, nearly 40 percent of FHWA Region 6 bridges are currently at or have exceeded their original design lives. Figure 2-3(a) shows the ages of stringer/multi-girder bridges within region 6 having a high daily truck traffic. These bridges have a functional classification of Principal Arterial as defined by the FHWA and are generally located along an interstate, freeway, expressway or another major roadway. Figure 2-3(b) shows the status of the principal arterial bridges.

From Figure 2-3(a), 60 percent (40 years of age or greater) of principal arterial bridges are nearing or have exceeded their original design life. With ever increasing traffic, fatigue damage rates will likely increase.

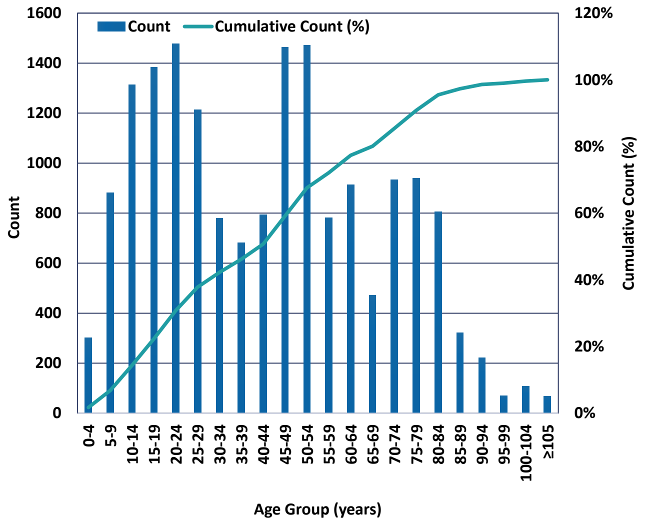

Figure 2-2: Age of Steel Highway Bridges in Region 6

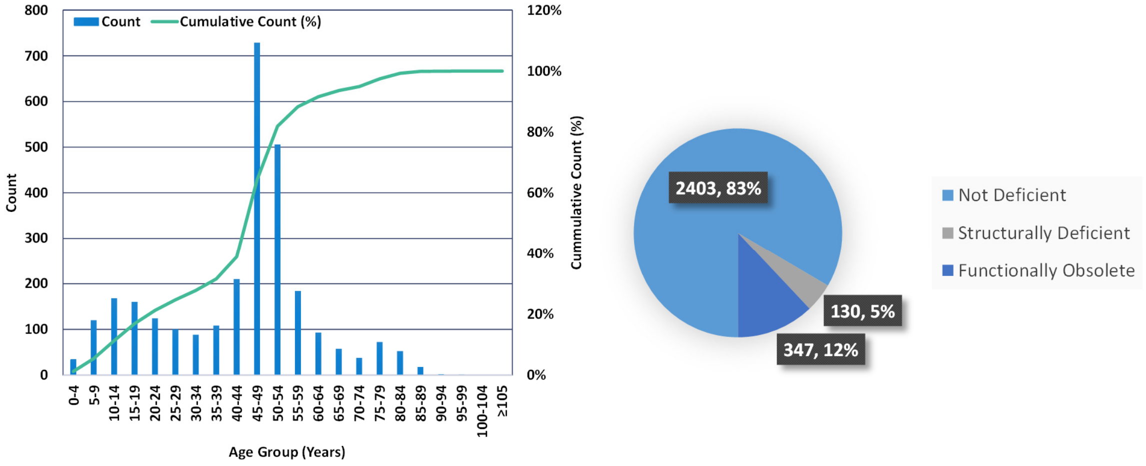

(a) (b)

Figure 2-3: (a) Age of Principal Arterial Multi-Girder Bridges in Region 6.
(b) Status of Principal Arterial Bridges in Region 6

2.2. *Influence of Corrosion Fatigue*

Corrosion-fatigue is simply characterized as fatigue in a corrosive environment. The combined influence of alternating stresses and an aggressive environment causes fatigue failure to occur at lower stress ranges and a lower number of cycles than fatigue in non-corrosive environments (Gangloff, 2005). Figure 2-4 shows two S-N curves for a typical metal in both air and seawater. In a corrosive environment the stress level associated with infinite life is lowered or completely removed; therefore there is no fatigue limit in a corrosion-fatigue setting.

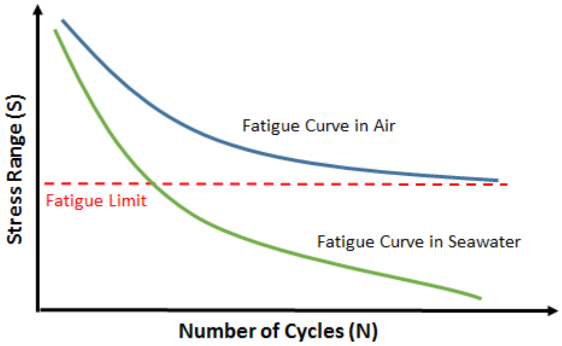

Figure 2-4: S-N Curve for typical metal in air and in seawater.

Corrosion fatigue damage typically accumulates in four stages: (1) cyclic plastic deformation, (2) micro-crack initiation, (3) small crack growth to linkup and coalescence, and (4) macro-crack propagation (Gangloff, 2005). The damage mechanisms associated with corrosion fatigue are dependent upon a variety of metallurgical and environmental (thermal and chemical) factors (hydrogen embrittlement; film rupture, dissolution, etc.); however, control of corrosion fatigue can be accomplished by either lowering the cyclic stresses or reducing stress concentrations in the structural components. More information on corrosion fatigue can be found in Gangloff (2005).

2.3. *Review of Fatigue Retrofit Methods*

In order to mitigate fatigue damage, localized repair and retrofitting techniques can be used to redistribute stresses within structural components while reducing stress concentrations. Many different techniques are used to repair fatigue cracks or retrofit critical fatigue details, including weld surface treatments, hole-drilling, installation of splice plates, and post-tensioning (Dexter & Ocel, 2013). A brief description of each of these techniques is discussed below. A more detailed discussion of other common repair and retrofit methods can be found in Dexter & Ocel (2013).

2.3.1. Weld Surface Treatment

Weld surface treatments are intended to increase the fatigue resistance of un-cracked welds by improving the geometry around the weld toe. Weld surface improvements may include reshaping by grinding, gas tungsten arc (GTA) re-melting, and impact treatments as described below. When the weld surface treatment is done properly, the fatigue life can be reset, implying that the effects of fatigue damage are completely removed (Dexter & Ocel, 2013).

Grinding: Eliminates small cracks by removing (grinding away) a small amount of structural material.

Gas Tungsten Arc: Cracks are repaired by re-melting the metal along the weld without adding new filler material.

Impact Treatments: Reduces the effective tensile stress range by introducing residual compressive stress near the weld toe. Figure 2-5 shows the result of an impact treatment on a weld toe

Figure 2-5: Impact treatment and geometry improvement of a weld toe (Dexter & Ocel, 2013)

2.3.2. Hole-Drilling in Steel Components

Hole-drilling involves making a through thickness hole into a structural component at the tip of a crack to prevent propagation. The drilled hole helps to lessen the stress concentration at the crack tip by redistributing the stresses in the structural detail. Hole diameters must be large enough to successfully arrest the crack and are typically in the range of 2 to 4 inches for steel structures (Dexter & Ocel, 2013). In addition to being the correct size, the hole must also be positioned properly so that the crack tip is contained. Figure 2-6 pictures the hole-drilling method and identifies the best location to position the hole.

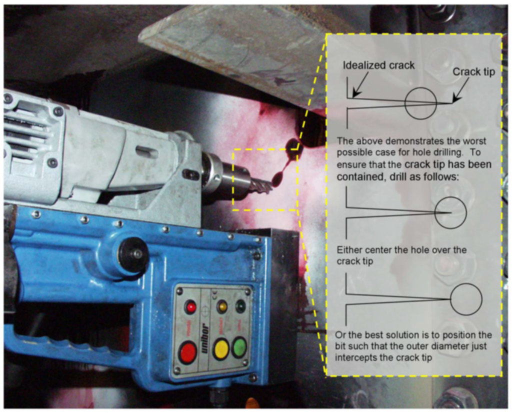

The above demonstrates the worst possible case for hole drilling. To ensure that the crack tip has been contained, drill as follows:

Either center the hole over the crack tip

Or the best solution is to position the bit such that the outer diameter just intercepts the crack tip

Figure 2-6: Hole-drilling and proper positioning for crack containment (Dexter & Ocel, 2013)

2.3.3. Splice Plates

Splice plates are often used as a repair method to provide continuity to a cracked section. They can also be used to restore strength to corroded elements. The concept of the splice plate is to increase the cross sectional area of a component which consequently reduces locally applied stress ranges. Figure 2-7 shows an example of a splice plate repair. The dotted line represents the crack growth beneath the splice plate while the circle shows the location of the hole drilled to remove the crack tip. Splice plates can be installed by welding or through the use of high strength bolts. According to the AASHTO specifications, a bolted connection may be considered as a category B detail, while a welded connection may result in a category D or E condition; indicating that a bolted connection has higher fatigue resistance (AASHTO, 2012)

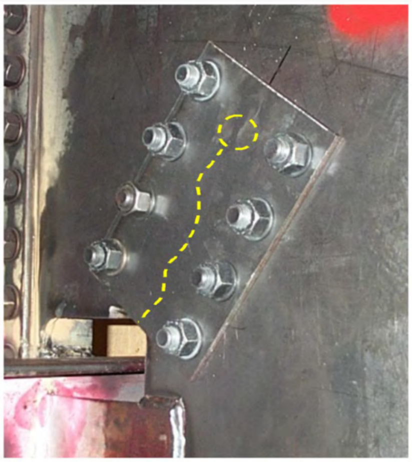

Figure 2-7: Splice Plate installed using high strength bolts (Dexter & Ocel, 2013)

2.3.4. Post-Tensioning

Post-tensioning is a repair or retrofit strategy intended to reduce tensile stresses around fatigue prone regions. In order for fatigue cracks to propagate, the crack must be able to open and close as alternating stresses are applied to the structure. Post-tensioning is a crack closure technique that introduces initial compressive stresses to an element, shifting the applied stress range into a more compressive regime.

Several options are available for applying post-tensioning forces including the use of pre-stressing strands, post-tensioning bars, or high strength threaded rods; however, proper corrosion protection must be applied to the system to ensure long term durability (Dexter & Ocel, 2013). Post tensioning is the retrofit strategy that will be used in this thesis using CFRP as the post-tensioned or pre-stressed material. Compared to typical post tensioning material (strands, bars, or threaded rods) made of steel, CFRP is corrosion resistant and contains other properties that make it an ideal retrofit material.

2.4. *Overview of CFRP and Review Applications in Structural Retrofits*

CFRP has a high strength-to-weight ratio which makes it viable for a wide range of applications. Several types of CFRP exist with varying elastic moduli and tensile strengths which further broadens the use of CFRP. Table 2-2 shows the five types of CFRP available.

Today, CFRP is used in the development of aircrafts, automobiles, sporting goods, and infrastructure systems. In concrete structures, CFRP has proven to be an effective retrofit material by restoring the strength of weakened components. In concrete, thin CFRP sheets are often wrapped around concrete structures in order to improve tensile strength, restrict buckling, or improve the ductility of components that have lost mass due to deterioration.

Table 2-2: Types of CFRP bases on modulus of elasticity and tensile strength (Kopeliovich, 2012)

Ultra High Modulus (UHM)	Modulus of elasticity:	> 65400 ksi (450 GPa)
High Modulus (HM)	Modulus of elasticity:	51000-65400 ksi (350-450 GPa)
Intermediate Modulus (IM)	Modulus of elasticity:	29000-51000 ksi (200-350 GPa)
High tensile, Low Modulus (HT)	Tensile strength:	> 436 ksi (3 GPa)
	Modulus of elasticity:	< 14500 ksi (100 GPa)
Super High Tensile (SHT)	Tensile strength:	> 650 ksi (4.5 GPa)

CFRP use in steel structures is a more recent application and has not yet been widely used in construction. Figure 2-8 compares the stress strain curve of mild steel and CFRP. As shown in Figure 2-8, CFRP has an elastic modulus similar to mild steel but much greater ultimate strength. This property contributes to the fatigue resistance of CFRP by enabling it to withstand greater mean stresses and stress amplitudes than steel. The corrosion resistance of CFRP makes it ideal for repair and retrofit efforts in steel structures, while its high strength to weight ratio (less than 1/3 weight of steel) allows it to add considerable strength and negligible weight to a component. One limiting property of CFRP is that it exhibits a brittle state of failure due to the lack of a well-defined yield point. In design, a safety factor is used to account for the brittle nature of the material.

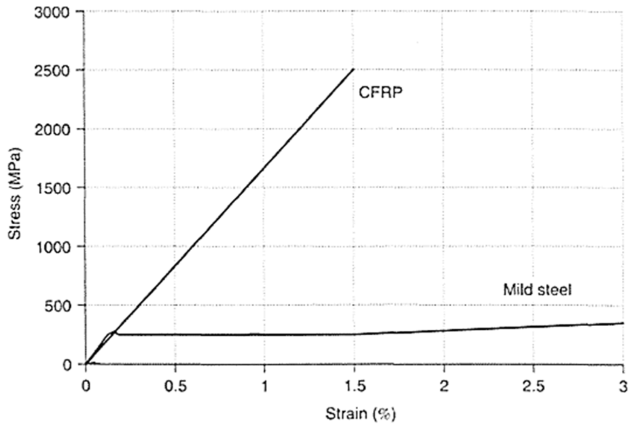

Figure 2-8: Stress-Strain curve for CFRP and Mild Steel (Teng et al., 2002)

Although CFRP is not a commonly used retrofit material for steel structures, it has been shown to improve the flexural strength and fatigue performance of steel components in several studies [Peiris & Harik (2015), Schnerch & Rizkalla (2008), Miller et al. (2001), Kaan et al. (2012), Huawen et al. (2010), Ghafoori et al. (2015)]. Flexural strengthening of steel components typically involves reinforcing tensile components subjected to bending, while fatigue strengthening involves reducing the applied stress range or mean stress in structural elements. In both cases the installation of CFRP on critical details helps to limit strains, therein reducing the stresses in structural details.

Fatigue testing is often performed under fully reversed loading with an applied mean stress of zero; however, in many real-life fatigue applications the mean stress is non zero. Some fatigue analysis procedures that account for the mean stress correction include the Goodman, Gerber, Morrow, and Soderberg models. The fatigue analysis model that will be used in this work is the Goodman approach. This method will be discussed further in 3.3.2, but is demonstrated in a recent research study by Ghafoori et al. (2015). In Ghafoori et al. (2015), a riveted steel railway bridge was retrofitted with un-bonded pre-stressed CFRP plates. The retrofit system was developed where CFRP plates are eccentrically applied to the bridge girder, and a pre-stress was applied to the CFRP to shift the mean stress of the bridge component into a state of infinite fatigue life. Similar to other reported data, this study shows that applying a pre-stress to CFRP material greatly increases the effectiveness of the retrofit. CFRP pre-stress level and thickness are two key parameters that influence the performance of the retrofit.

In this thesis a localized retrofit using pre-stressed CFRP strips is developed to reinforce critical fatigue details within steel bridge components. As indicated in the AASHTO specifications, critical fatigue details are commonly located near welded joints. The retrofit developed in this study will focus on critical components near welded and bolted connections seen in steel stringer/multi-girder bridges within region 6.

3. Analytical Investigation into Steel Bridge Component Fatigue

3.1. *Selection of Bridges for Analysis*

3.1.1. Identification of Common Bridge Types

A variety of steel bridge construction types (stringer/multi-girder, truss, culvert, arch, suspension, etc.) exist within region 6; however, stringer/multi-girder construction types are the most common. Figure 3-1 shows the frequency of steel highway bridge construction types within region 6. Note that only the ten most frequent construction types are shown. Stringer/Multi-girder bridges make up 13,361 (76.7%) of the 17,400 total steel highway bridges in the region 6. With the highest quantity of constructed brides being of stringer/multi-girder construction, and in order for the retrofits to have the greatest impact, it was decided to consider only stringer/multi-girder type constructions in this study.

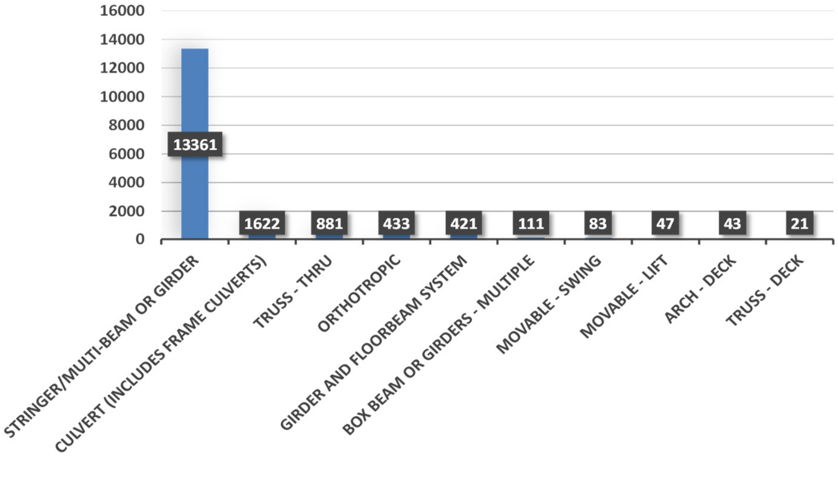

Figure 3-1: Frequency of region 6 steel highway bridge construction types

3.1.2. Chosen Designs for Study Models

Bridges chosen for this study are aimed to be representative of the stringer/multi-girder construction within region 6. Stringer/Multi-girder steel bridges can generally be classified by geometry (skew or non-skew), cross-frame configuration (diaphragm or cross-frame), and support conditions (simply supported or continuous). Four region 6 bridges containing a combination of these design features are evaluated in this work. In addition to these construction details, the selected bridges also vary in span length to determine the effect of span length on the location of critical fatigue regions. All of the selected bridges have a functional classification of principal arterial (interstate, freeway, expressway or other major roadway) to ensure that this study is relevant to bridges that are frequently travelled. Table 3-1 summarizes the construction details for each of the bridges evaluated in this study.

Table 3-1: Construction Details for Selected Bridges.

State	Name	Length (ft)	No. Long. Girders	No. of Spans	Lanes	Cross-Frame Config.	Skew	Span Type
AR	A-3956	120	7	3 @ 40 ft	2	Diaphragm	None	Simply Supported
AR	A-3958	456	5	6 @ 76 ft	2	Diaphragm	30°	Simply Supported
TX	T-130	130	5	Cont.	2	Cross- Frame	None	Continuous
AR	A-6243	240	5	Cont.	2	Cross- Frame	44°	Continuous

3.2. *Modeling Techniques*

3.2.1. Geometry/Element Type

Construction documents for each bridges evaluated in this work were provided by state DOTs within region 6. Detailed three-dimensional (3D) models simulating the geometry of each bridge were developed using ABAQUS. The global boundary conditions of the bridge models simulate the support conditions seen in the constructed bridge. Four-node linear shell elements were used to model all geometries and connection regions. Shell elements provide analytical results for the top and bottom face of each element, while solid elements provides analytical results through the thickness of the element. Shell elements were used in the analysis to reduce the computational cost.

While the simulated bridge connection regions assume a rigid (zero rotation) assembly, actual bolted connections within the bridge may act semi-rigid joints (allowing small rotations). Bolted regions within the cross-frame configurations were excluded from all models for simplicity.

Mesh size can affect the accuracy and computational expense of the finite element analysis. Typically, smaller element size is associated with greater accuracy and higher computational expense. The general mesh size used for bridges A-3958, T-130, and A-6243 is 2in x 2in. A smaller mesh size of 1 in. is used for bridge A-3956 because the girder cross-section is much smaller (W21 vs. W30, W36, and W48). These mesh sizes allow for 15 to 25 elements within the beam web height.

The bridges were analyzed statically using a linear equation solver. The linear solver uses a sparse, Gauss elimination method where the storage of equations occupies a large portion of the disk space during the calculations (SIMULIA, 2012). Table 3-2 shows the number of elements and nodes considered in the analysis, as well as the number of equations and approximate computational time necessary to complete the analysis. Not surprisingly, the computation time increases significantly as both the model size increases, and the element size decreases. Computational time was further reduced on the simply supported bridges (A-3956, and A-3958) by considering only one span length. Note that the computational time also depends on the number of processes running and the computer memory available.

Table 3-2: Number of elements, nodes, equations, and computational time for static analyses

Bridge	Span Length	Typical Element Size	No. of Elements	No. of Nodes	No. of Equations/Unknowns	Comp. Time
A-3956	40 ft.	1 in.	156,727	160,234	956,952	2.92 hrs.
A-3958	76 ft.	2 in.	78,533	80,966	484,176	2.17 hrs.
T-130	130 ft.	2 in.	140,190	146,008	873,528	5.50 hrs.
A-6243	240 ft.	2 in.	384,814	403,546	2,377,992	31.90 hrs.

A picture and description of each bridge is given below along with the bridge model showing the cross-frame configuration, and typical element mesh size used during the analysis.

Bridge A-3956

Bridge A-3956 is pictured in Figure 3-2(a). This bridge was constructed in 1968 and services Interstate-540 and crosses over Flat Rock Creek near Van Buren, Arkansas. The ABAQUS model, diaphragm details and mesh size for bridge A-3956 are shown in Figure 3-2(b). Bridge A-3956 is non skewed and carries two lanes of vehicular traffic along three simply supported spans of 40 ft. This bridge was classified as structurally deficient in the 2013 NBI database. The seven longitudinal girders (W21x62) are spaced at 6’-3” and contain cover plate attachments welded to the bottom flanges. Longitudinal girders are connected by one row of C shape diaphragms (C12x20.7) bolted to steel gusset plates (not-shown), then welded at the girder mid-span.

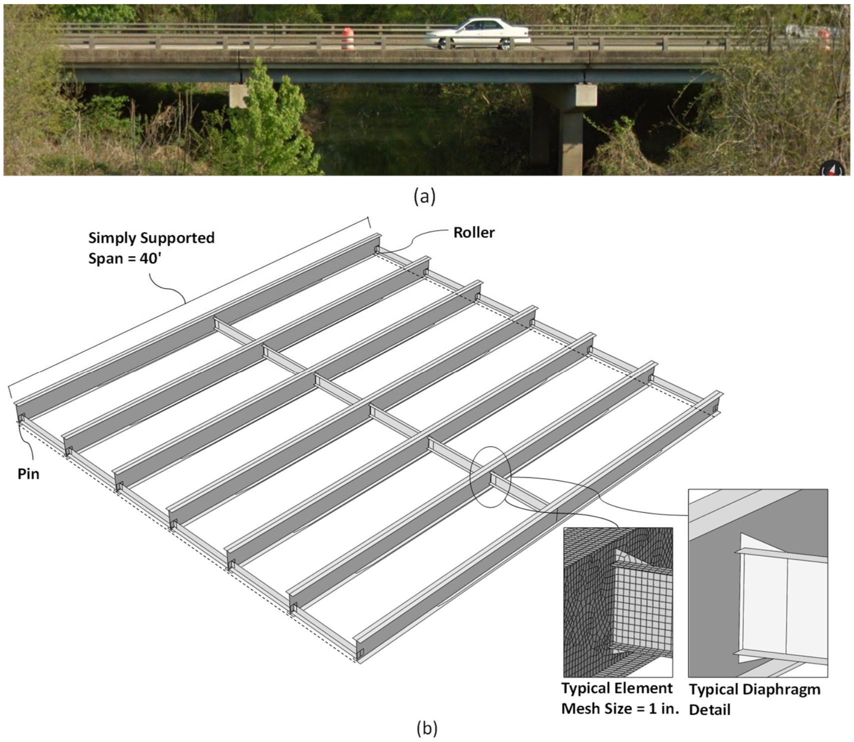

Figure 3-2: Bridge A-3956 (a) elevation picture (Google Maps) (b) ABAQUS model

Bridge A-3958

Bridge A-3958 is pictured in Figure 3-3(a). Bridge A-3958 was also constructed in 1968. This bridge was classified as structurally deficient in the 2013 NBI database and was recently reconstructed in 2014. The analysis of this bridge is based on the design prior to reconstruction; however, the results of this study will be applicable to the many existing bridges that have an identical or similar design. The bridge services Interstate-540 and crosses over a railroad track near Van Buren, Arkansas. The ABAQUS model, diaphragm details and mesh size for bridge A-3958 are shown in Figure 3-3(b). Bridge A-3958 has a skewed geometry and carries two lanes of vehicular traffic along six simply supported spans of 76 ft. The five longitudinal girders (W36x160) are spaced at 6'-6" and contain cover plates attachments welded to the bottom flanges. Longitudinal girders are connected by C shape diaphragms (C15x33.9) staggered along the span. Diaphragms are bolted to steel plates (not-shown), then welded at the girder mid-span.

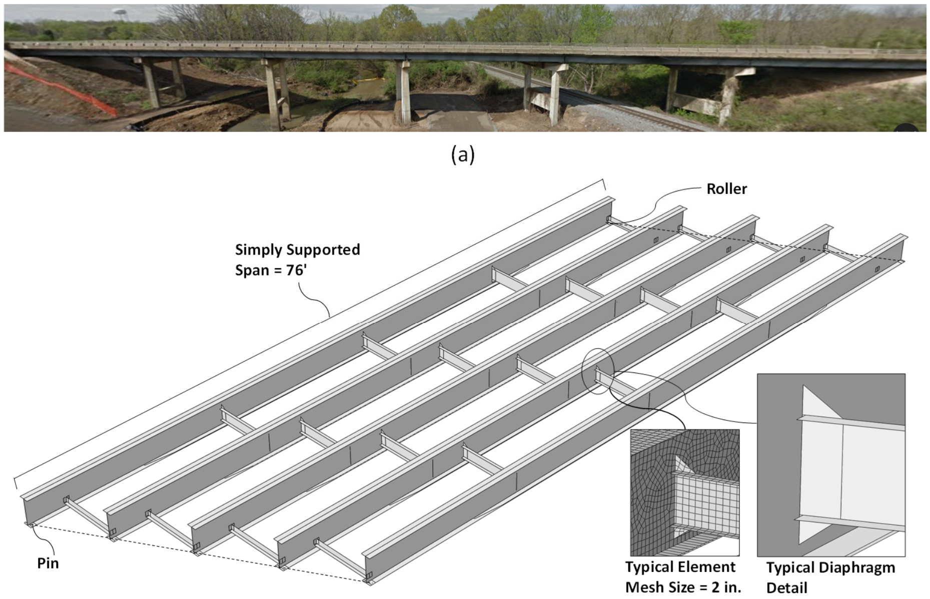

(a)

(b)

Figure 3-3: Bridge A-3958 (a) elevation picture (Google Maps) (b) ABAQUS model

Bridge T-130

Bridge T-130 is pictured in Figure 3-4(a). Bridge T-130 was constructed in 1968 and was classified as functionally obsolete in the 2013 NBI database. The bridge services Interstate-35 and crosses over Highway-56 Creek near Moore, Texas. The ABAQUS model, diaphragm details and mesh size for bridge T-130 are shown in Figure 3-4(b). Bridge T-130 is non skewed and carries two lanes of vehicular traffic along a continuous span of 130 ft (40~50~40). The bridge is pinned at the two interior supports and contains expansion shoes (rollers) on both ends of the structure. The five longitudinal girders (W30x108) are spaced at 9'-0" and contain cover plate attachments welded to the top and bottom flanges above the interior supports. Longitudinal girders are connected by three types of cross-frames: Cross-Frame details A and B (shown in Figure 3-4(b)) are installed alternatively along the bridge span. The third cross-frame detail is located above the two end supports; the stresses in this detail are minimal, therefore, the close up detail is excluded from Figure 3-4(b). Cross frame details A and B are both welded to the longitudinal girders. Detail A consists of three L-shapes welded in an "X" configuration, while detail B consists of one T-shape and three L-shapes welded in a "K" configuration.

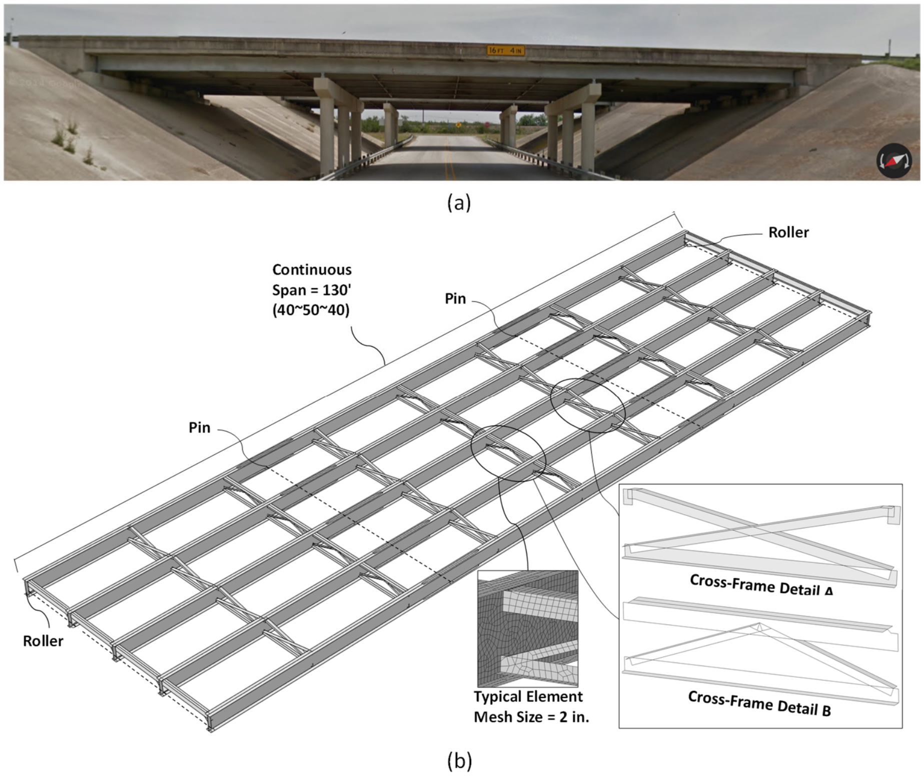
(a)
(b)

Figure 3-4: Bridge T-130 (a) elevation picture (Google Maps) (b) ABAQUS model

Bridge A-6243

Bridge A-6243 is pictured in Figure 3-5(a). Bridge A-6243 was constructed in 1994 and was given a not-deficient status in the 2013 NBI database. This bridge is located along Interstate-49 and crosses over Highway-265. The ABAQUS model, diaphragm details and mesh size for bridge A-6243 is shown in Figure 3-5(b). The bridge has a skewed construction and carries two lanes of vehicular traffic along a continuous span of 240 ft (70~100~70). The bridge is fixed at the center supports and contains expansion shoes (rollers) on both ends of the structure. The five longitudinal built-up plate girders have a web depth of 48 in., flange width of 12 in., and are spaced at 9’-0”. Transverse stiffeners are welded to the web of the longitudinal girders at the location of each cross-frame. The cross-frames (shown in Figure 3-5(b)) are made up of four L-sections that are welded to gusset plates then bolted (not shown) to the web stiffeners.

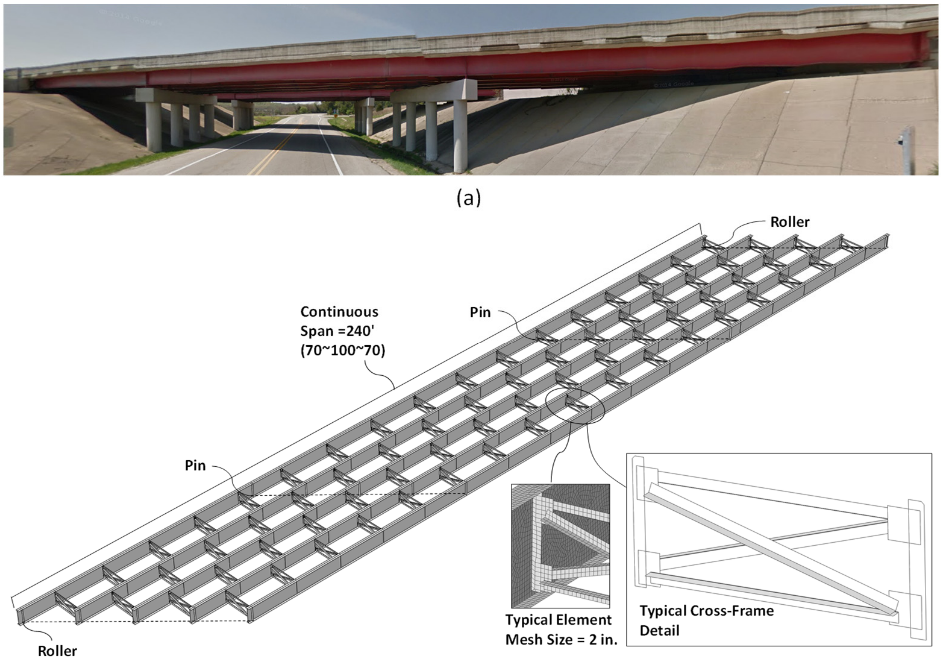
(a)

(b)

Figure 3-5: Bridge A-6243 (a) elevation picture (Google Maps) (b) ABAQUS model

3.2.2. Materials & Loading

Because the fatigue loadings occur under service loadings, elastic steel material properties are used in the ABAQUS analysis. Typical values of Young's modulus (E=29000 ksi) and Poisson's ratio (ν=0.3) were considered in the model.

The AASHTO fatigue truck served as the loading condition for each of the bridge models. The characteristics of the fatigue truck are shown in Figure 3-6. The fatigue truck consists of an 8,000 lb. front axle spaced 14 ft from the 32,000 lb. mid axle, with the mid axle spaced 30ft. from the 32,000 lb. rear axle. As indicated in the 2012 AASHTO specifications, a dynamic load allowance factor (IM) of 1.15 is applied to each axle weight to account for wheel load impact from moving vehicles. Additionally, a fatigue load factor (γ) of 1.5 is applied to each of the axle weights in order to analyze the bridges using the AASHTO Fatigue I load combination (infinite fatigue life) (see 2.1).The global models were also analyzed using hypothetical load factors of 1.65, 1.75, 1.85, and 2.0 (total of five analyses per bridge) in order to determine the effect of increased traffic loads on the local stress range and overall fatigue performance of bridge components.

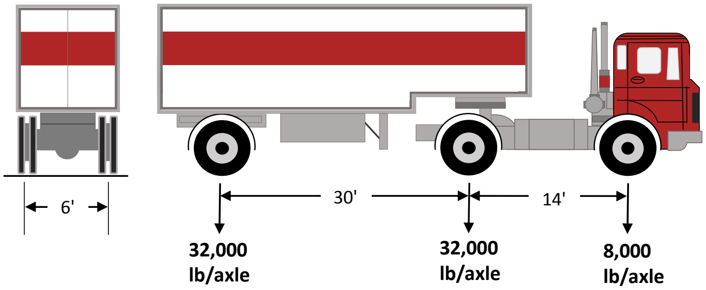

Figure 3-6: Characteristics of the AASHTO fatigue design truck HS 20-44

All of the models were loaded with the assumption that the fatigue truck was traveling in the right vehicular lane. The truck loading was divided amongst the girders supporting the traffic lane based on the tributary area of the girders. Figure 3-7 shows a schematic of the bridge lanes and girders for bridges T-130 and A-6243. As shown in Figure 3-7, the truck travels between girders C and D when driven in the right lane. Based on the tributary area for each girder, the wheel loads were divided equally between girders C and D in the ABAQUS model. Note that bridges A-3956 and A-3958 have a different lane layout and girder spacing, therefore, the load is applied differently. All of the brides have a lane width of 12 ft., however, bridges A-3956 and A-3958 have a girder spacing of 6’-3” and 6’-6” respectively. Due to the shorter girder spacing and the change in bridge layout, the right traffic lane is supported by three consecutive girders. Based on this configuration, the middle of the three girders carries twice the load (1/2 of axle weight) of the outer two girders (1/4 of axle weight each).

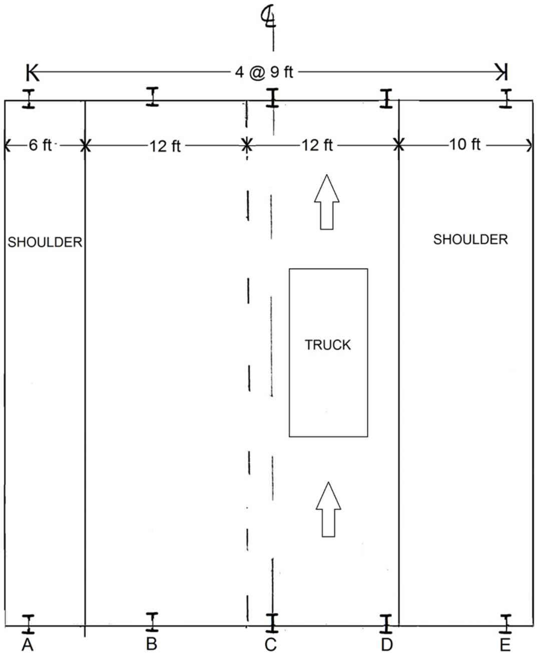

Figure 3-7: Schematic of bridge lanes and girders for bride A-6243 and T-130

Sequences of statically applied loads simulate the truck passage along the bridge span. Figure 3-8 shows the truck wheel loading scheme used in the ABAQUS models. Vertical loads corresponding to the individual wheel loads are activated and deactivated in series to simulate a moving load. The process of activating and deactivating are overlapping such that the ramping up coincides with the ramping down of the previous load. The load increments are spaced at 6 in. along the entire bridge span for all of the bridge models.

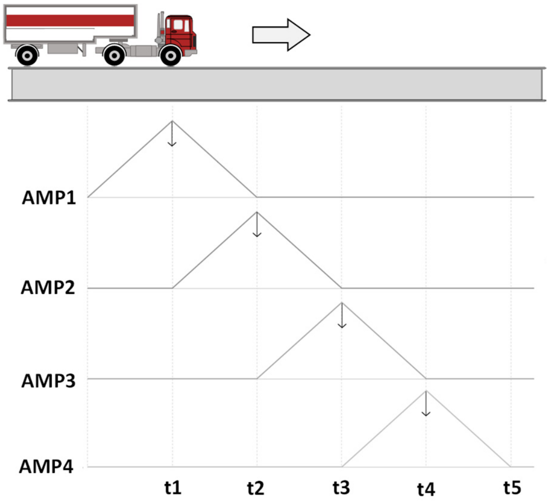

Figure 3-8: Wheel loading scheme

3.3. *Determination of Fatigue Damage*

This section discusses the approach used to analyze the fatigue damage in critical bridge components.

3.3.1. Miner's Total Damage

Miner's rule is a commonly used cumulative damage model to evaluate fatigue performance in structural components. In Miner's total damage approach, fatigue damage is inversely proportional to the fatigue capacity at each applied stress range; furthermore, higher stress ranges result in greater fatigue damage. Miner's rule is shown in Equation 3-1

$$\sum \mathrm{D_i} = \sum \frac{\mathrm{n_i}}{\mathrm{N_i}} \qquad \text{Equation 3-1}$$

where D_i, n_i, and N_i are the damage, number of cycles and number of cycles to failure for each applied stress range, i. Ni is given by Equation 3-2

$$N_i = A(\Delta\sigma)^{-3} \qquad \text{Equation 3-2}$$

where A is the detail category constant (see Table 2-1) and $\Delta\sigma$ is the applied stress range. The individual cycles, n_i, and the applied stress range, $\Delta\sigma$, are determined using the rain-flow cycle counting procedure described in Appendix A.

In this work, Miner's rule is used to determine the location of bridge details susceptible to fatigue damage. The stress histories in bridge details are determined using ABAQUS and the resulting fatigue damage is compared for various locations along the span.

3.3.2. Modified Goodman Fatigue Analysis

The AASHTO steel bridge specification considers stress range (S-N curve) as the main parameter to evaluate fatigue. The modified Goodman criterion criteria provides a more accurate fatigue assessment by considering the localized effects of mean stress, stress amplitude, and the steel material properties. For a given stress cycle, the mean stress (σ_m) and the stress amplitude (σ_a) are expressed by Equation 3-3 and Equation 3-4

$$\sigma_m = \frac{\sigma_{max}+\sigma_{min}}{2} \qquad \text{Equation 3-3}$$

$$\sigma_a = \frac{\sigma_{max}-\sigma_{min}}{2} \qquad \text{Equation 3-4}$$

where σ_{max} and σ_{min} are the maximum and minimum stresses in a given stress history. A sample stress history denoting the variables the σ_m, σ_a, σ_{max}, and σ_{min}, is shown in Figure 3-9(a). Figure 3-9(b) show a constant life diagram (CLD) representing the modified Goodman criteria. The modified Goodman line is represented by a straight line acting through σ_a=S_e and σ_m=S_{ut}. S_e and S_{ut} are the fatigue endurance limit and ultimate tensile strength of the material, respectively. The Goodman line is given by Equation 3-5

$$\frac{\sigma_a}{S_e} + \frac{\sigma_m}{S_{ut}} = \frac{1}{n} \qquad \text{Equation 3-5}$$

where n is a factor of safety. A procedure for calculating S_e is presented in (Shigley, 1989). For steel, the endurance limit can be estimated as

$$S_e' = \begin{cases} .5\, S_{ut} & S_{ut} \le 200ksi \\ 100\; ksi & S_{ut} > 200ksi \end{cases} \qquad \text{Equation 3-6}$$

The prime mark on S'_e refers to rotating-beam specimens prepared and tested in laboratory conditions. It is unreasonable to expect the actual endurance limit of a structural material, S_e, to match the values obtained in laboratory conditions; therefore, Marin (1962) identified factors to quantify the effects of surface conditions, size, loading, temperature and miscellaneous items. The Marin equation is given by

$$S_e = k_a k_b k_c k_d k_e k_f S_e' \qquad \text{Equation 3-7}$$

where k_a, k_b, k_c, k_d, k_e, and k_f, are respectively, the surface condition, size, load, temperature, reliability, and miscellaneous effects modification factors. The procedure to calculate S_e, and the Marin factors is shown in Appendix B.

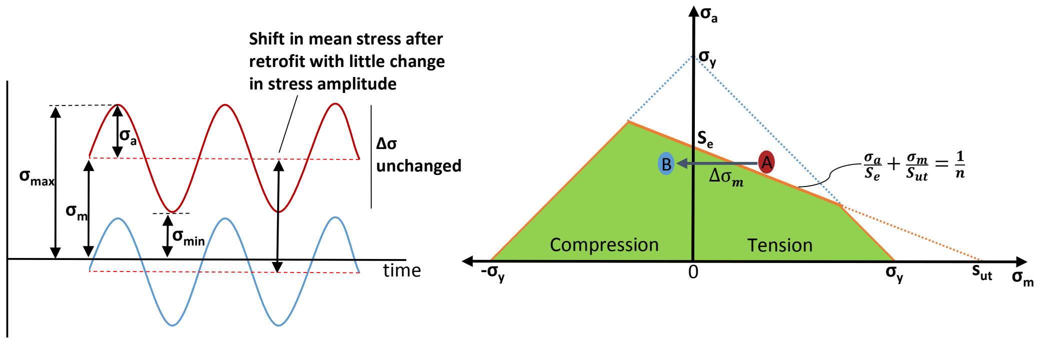

Figure 3-9: (a) Sample stress history (b)CLD representing the modified Goodman criteria

Using the modified Goodman criteria, a value σ_m and σ_a corresponding to a location above the curve is representative of finite fatigue life, where as a location below the curve is indicative of infinite fatigue life (safe region). A detail that contains finite fatigue life (point A in Figure 3-9(b)) can be shifted to a state of infinite fatigue life (point B in Figure 3-9(b)), by either reducing the stress amplitude or reducing the mean stress. Reducing the stress amplitude of critical fatigue details may require adjustments to the cross-section (hole-drilling, splice plates, etc.) or the loading conditions; however, reducing the mean stress can be achieved through post tensioning techniques by shifting the stress range into a more compressive regime. Figure 3-9(a) shows the shift in mean stress with Figure 3-9(b) illustrating the corresponding shift on the Goodman diagram. The retrofit developed in this work utilizes pre-stressed CFRP strips to reduce the mean stress of bridge details into the safe region, extending the component life indefinitely.

4. Results and Discussion from Model Analyses

4.1. *Validation of Modeling Techniques*

In addition to the evaluation of the four bridges described earlier, a validation study is included in this work to verify that the modeling techniques used are satisfactory. The validation study is conducted on bridge A-6243, and uniaxial strain gauges are installed on the actual bridge superstructure to record strain measurements for comparison with results from the FEM analysis. Figure 4-1 shows a picture of the (a) actual cross-frame compared with the (b) modeled cross-frame. The dimensions of the model closely match the actual dimensions of all the structural components, as they were taken from the actual design drawings.

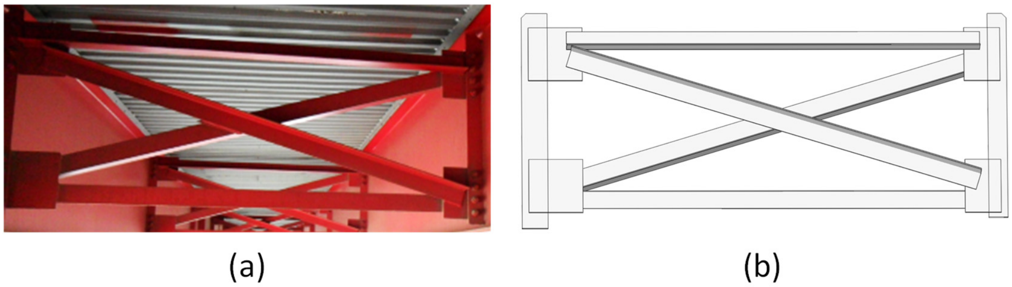
(a)
(b)

Figure 4-1: (a) Actual cross-frame detail (b) Modeled cross-frame with rendered shell thickness

The bridge was instrumented with three uniaxial strain gauges. Figure 4-2 shows the location and a picture of each of the installed strain gauges. Gauge 1 is located on the central girder below the cross frame detail approximately 23’ from the end support of the structure. Gauges 2 and 3 are located on the bottom of the tension flange of the central girder approximately 32’-7” from the end support. In order to obtain accurate and precise strain measurements, the installation surface is typically cleaned and prepared prior to bonding of the strain gauge, where the surface is stripped of any paints or coatings, then cleaned to remove stagnant dust particles. During this validation study however, the gauges were applied above the coated steel in an effort to preserve the corrosion protection on the bridge girders.

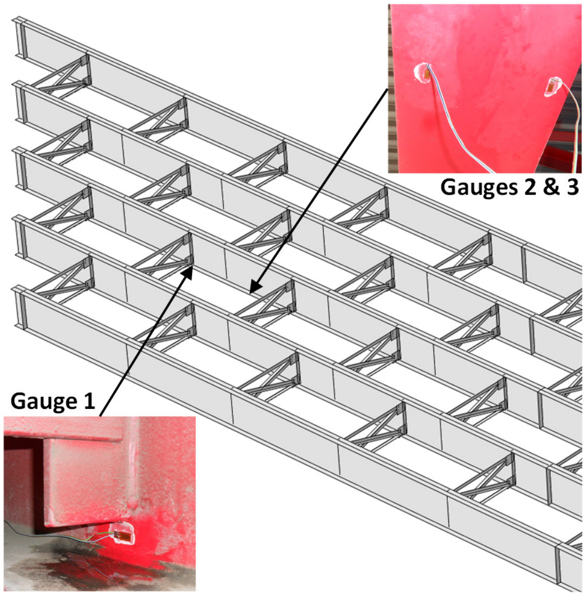

Figure 4-2: Location and picture of installed strain gauges

The University of Arkansas vibroseis truck served as the controlled traffic condition on the bridge. During the field test and FEM analysis, the truck was driven across the bridge in the right lane of the two lane bridge. A schematic of the lanes and location of the girders was shown previously in Figure 3-7. Figure 4-3 shows a picture of the vibroseis truck, axle spacing, and the individual wheel loads used in both the bridge loading and ABAQUS simulation. The two axles are spaced at 16’-6”. A wheel load of 3,800 lbs acts on both the driver and passenger front tires, while a wheel loads of 7480 lbs. and 7290 lbs. act on the rear driver and rear passenger tires, respectively.

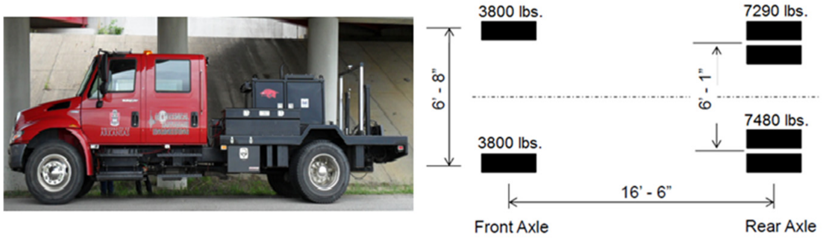

Figure 4-3: Vibroseis truck axle weights and individual wheel loads

In the validation study, the bridge is analyzed dynamically as opposed to statically in order to better simulate the truck passage when compared with the experimental readings. Table 4-1 shows the number of elements and nodes considered in the dynamic analysis, as well as the number of equations and approximate computational time necessary to complete the analysis. By specifying a larger element size of 3 in., the computation cost was reduced to about half the expense necessary for the static analysis. The dynamic analysis is conducted using the Hilber-Hughes-Taylor time integrator. The Hilber-Hughes-Taylor is an implicit integration approach where the operator matrix must be inverted, and a set of simultaneous nonlinear dynamic equations must be solved at each time increment; this solution is done iteratively using Newton's method (SIMULIA, 2012).

Table 4-1: Number of elements, nodes, equations, and computation time for dynamic analysis

Bridge	Span Length	Typical Element Size	No. of Elements	No. of Nodes	No. of Equations/Unknowns	Comp. Time
A-6243	240 ft.	3 in.	165,142	175,530	1,050,888	17.67 hrs.

Sequences of dynamically applied loads simulate the truck passage along the bridge span. Similar to the static analysis, where vertical loads corresponding to the individual wheel loads are activated and deactivated in series to simulate a moving load (see Figure 3-8); however, the dynamic analysis considers inertial effects and vibrations of the bridge from previous time-steps. Two percent Rayleigh damping from the first and second vibration modes was considered in the analysis.

A truck speed of 63 mph was recorded during the strain measurements and used in the dynamic analysis. Figure 4-4(a-c) shows the strain measurements recorded during the truck passage compared with the results of the FEM simulation for gauges 1, 2, and 3, respectively. The recorded real-time strain data for each of the gauges is shown by the solid line, while the FEM results for the corresponding location is shown by the dotted line.

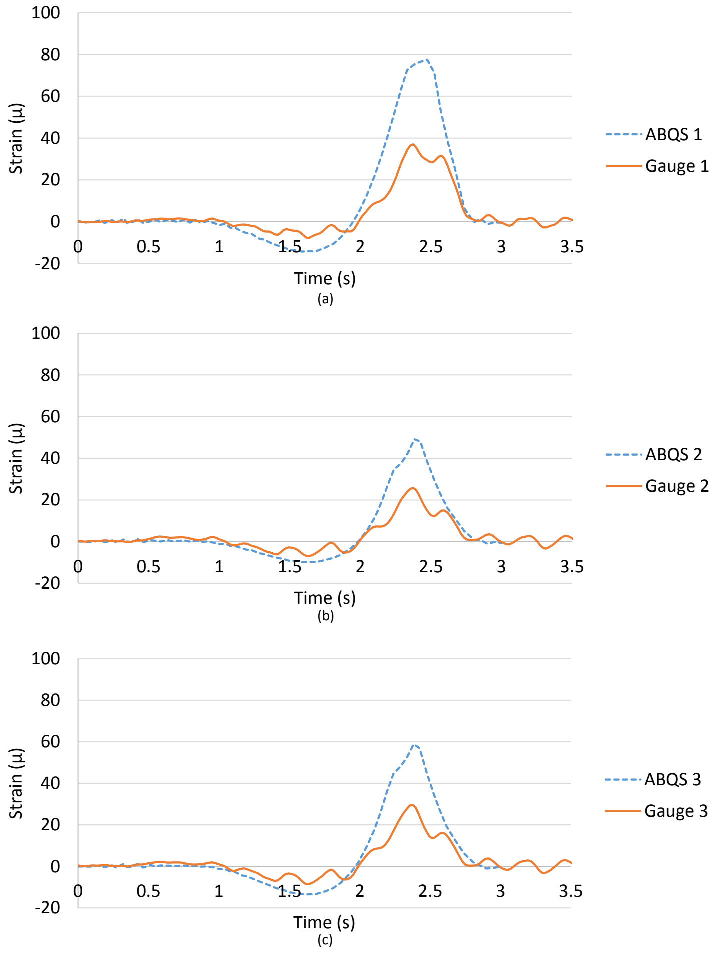

Figure 4-4: Comparison of strain gauge measurements with FEM results at (a) gauge 1, (b) gauge 2, and (c) gauge 3 locations

From Figure 4-4, the FEM results overestimate the strain values by about 20-40 μin/in for each of the strain gauge locations. This error may be the result of two primary modeling issues: (1) The concrete bridge deck was excluded from the FEM. The concrete deck may significantly increase the stiffness of the bridge section, consequently reducing the stain calculated in the bridge girders. It is important to note that the deformation are measured on a very small scale; therefore, a small change in the cross-section of structural elements may significantly affect the FEM analysis. Inclusion of the concrete deck also may have doubled the computational cost of the analysis. (2) The model assumes that the truck weight was distributed equally amongst the girders under the traffic lane. This assumption was made based on the tributary area of the girders supporting the traffic lane. In the actual structure the truck may not have been centered in the traffic lane, which may cause the load to be distributed unevenly to the girders. Additionally, the inclusion of a concrete deck may have helped to distribute the truck load to other girders. Some other causes of error may include the following:

Strain gauges were installed above the coated steel as opposed to being installed to the bare steel. A mesh and element size of 3 in. was used in the FEM analysis. This mesh can be further refined to produce more accurate results in local areas having higher strain gradients. Comparing the predicted and measured responses, it is determined that the ABAQUS model reasonably computed the local strains observed during testing.

4.2. *Determination of Critical Fatigue Regions*

In steel structures, critical fatigue regions typically occur near the welded connection of components. The presence of the weld creates concentrated stresses at the weld toe during loading cycles and can eventually initiate fatigue cracks. Figure 4-5 shows the von Mises stress distribution in bridge A-6243 when the truck is at mid-span. In this bridge, concentrated stresses can be seen in two locations: 1) welded connection between the transverse stiffener and top flange of the girder, and 2) welded connection between the bottom of the transverse stiffener and the girder web. For the four bridges analyzed in this work, locations with high stress concentrations are investigated further to determine the applied stress range and accumulated fatigue damage.

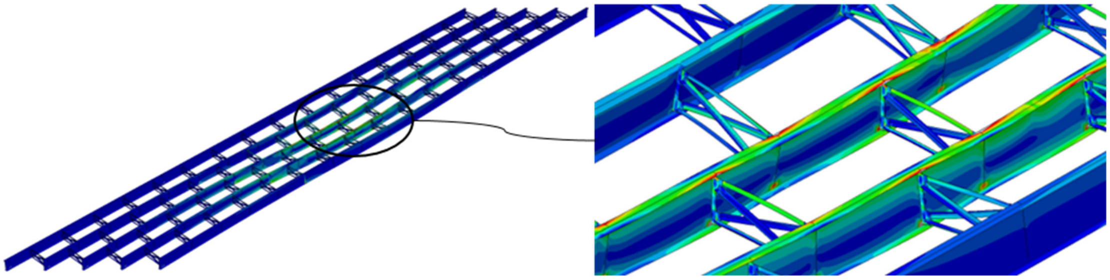

Figure 4-5: von Mises stress distribution at mid-span in bridge A-6243
(Note: Deflections are scaled 30 times)

To determine the location of critical fatigue components, stress cycles in structural details are compared at various locations along the bridge span. The bridge models were analyzed assuming a fatigue 1 load combination for five different load factors ranging from 1.5 (actual AASHTO fatigue 1 load factor) to 2.0 (hypothetical load factor). Various load factors are considered to determine the effect of an increased load on the local stress range and overall fatigue performance of the bridge detail.

Figure 4-6 shows the resulting stress cycles from the maximum in plane stress component due to the five considered load factors (1.5 1.65, 1.75, 1.85, and 2.0) and location of the details most susceptible to fatigue in each bridge. At least two structural details were identified for each bridge based on the stress range and detail category. As expected, the cross frame or diaphragm detail subjected to the highest stress range is located midway between supports for each bridge (see location 2, 5, 7, 8, and 9). These locations all contain welded connections between the bottom of the cross-frame configuration and the web of the longitudinal girder. Location 4 (see Figure 4-6(b)) is positioned on the opposite side of the weld between the diaphragm and the girder web. Due to the skewed bridge geometry, this location is subjected to distortion induced fatigue, where the girder web displaces laterally as well as vertically. This distortion can also be found in bridge A-6243 location 9 (see Figure 4-6(d)). Figure 4-7shows the distortion in the girder web of bridges (a) A-6243 and (b) A-3958 due to the skewed bridge geometry. Figure 4-7(b) illustrates how the distortion in the web creates tensile stresses on the opposite side of the diaphragm connection due to the lateral deflections in the web. Additionally, tensile stresses are present at the bottom of the diaphragm connection within the weld due to the downward deflection. In Figure 4-7(a), the transverse stiffener is welded to the top flange and the web of the girder which helps to lessen the lateral deflection near the top of the section; however, high stress concentrations are still present within the web at the bottom of the cross-frame detail due to lateral and downward deflections.

Locations 1, 3, and 6 show the stress history at the weld between the cover plate and the flange of the longitudinal girder. The stress history at location 6 (see Figure 4-6(c)) is within the top flange as opposed to the bottom flange because the detail is located over a negative moment region in the continuous span of bridge T-130. Finally, location 10 (see Figure 4-6(d)) show the stress history at the weld between the bearing stiffener and the flange of the girder. Similar to location 6, location 10 is also within a negative moment region, above the fixed support of bridge A-6243.

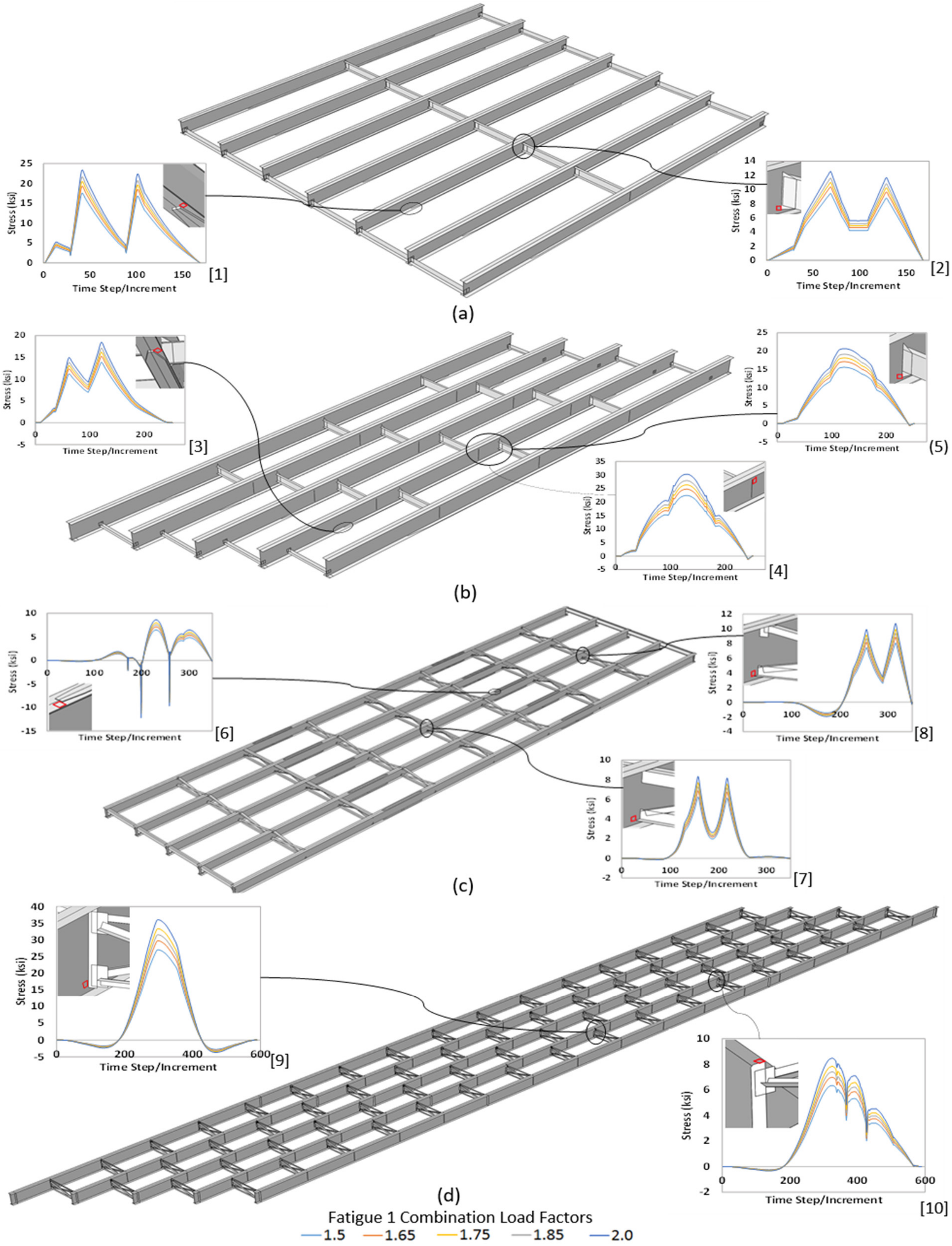

Figure 4-6: Stress history at structural details most susceptible to fatigue for bridges (a) A-3956, (b)A-3958, (c) T-130, and (d) A-6243

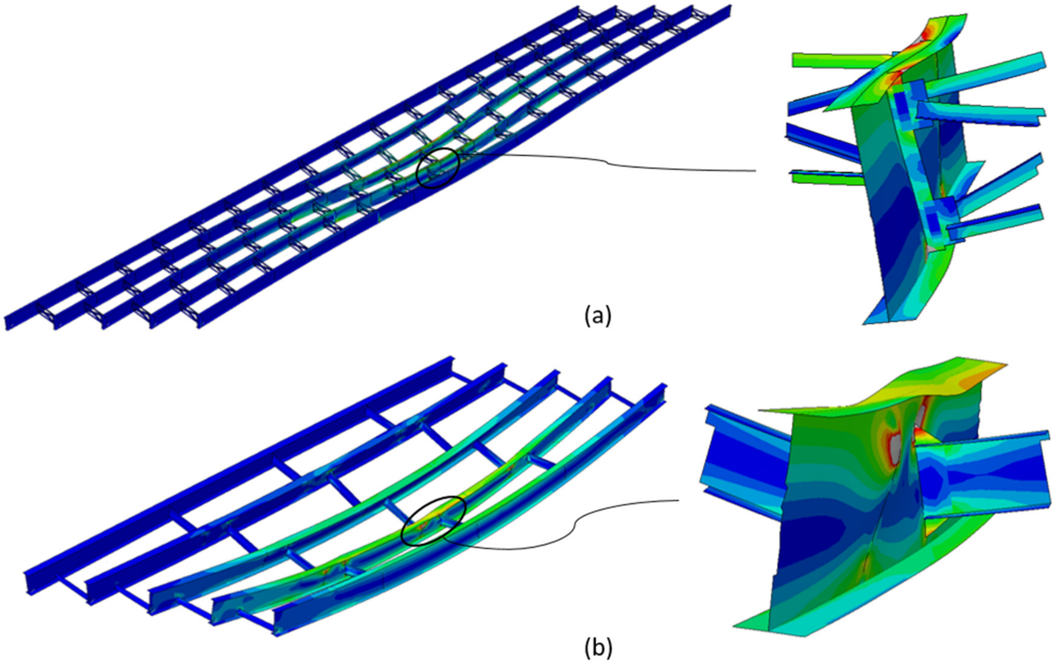

Figure 4-7: von Mises stress distribution showing distortion in the girder web of bridges (a) A-6243 and (b) A-3958 (Note: Deflections are scaled 50 times for visualization.)

The fatigue damage resulting from the different stress histories is determined through cycle counting using the rain-flow counting method (see Appendix A), and linear fatigue damage accumulation using Miner's rule (described in 3.3.1). Table 4-2 shows the resulting fatigue damage in the bridge details due to the stress histories shown in Figure 4-6 considering the 1.5 load factor. This calculation assumes that only 60% of the stress within the compressive region is damaging (Macdonald, 2011).

In Table 4-2, the largest fatigue damage within bridges A-3956, A-3958, and T-130 is found within the weld between the cover plate and girder flange (see locations 1, 3, and 6). This high fatigue damage is due to the low fatigue capacity associated with the cover plate connection (AASHTO detail category E) compared with the other detail categories. The remaining structural details (locations 2, 4, 5, 7, 8, 9, and 10) are all located at a cross-frame or diaphragm connections and contain stress ranges similar to or much greater than the cover plate details. These structural details contain much higher fatigue capacities according to the 2012 AASHTO specification are consistent with detail categories C' (location 2, 5, 9, and 10) or D (location 7 and 8), with the exception of location 4 which is identified as detail category A. Although the cross frame details are indicated as the fastest damage accumulation based on nominal stress data and the AASHTO detail categories, at a fundamental level fatigue performance is based on the mean stress and stress amplitude; therefore each location in Figure 4-6 is analyzed using the Goodman criterion to determine which details are not within the infinite fatigue life (safe) region.

Table 4-2: Fatigue damage calculations for critical structural details due to 1.5 load factor

Location[a]	Bridge	Stress Range [ksi]	Number of Cycles [n_i]	N_i[b]	Total Damage [ΣD]
1	A-3956	17.2	1	7.66E+04	2.07E-05
		2.1	1	4.21E+07	
		14.4	1	1.31E+05	
2	A-3956	9.2	1	5.65E+06	1.99E-07
		4.6	1	4.52E+07	
3	A-3958	13.7	1	1.52E+05	6.77E-06
		4.1	1	5.66E+06	
4	A-3958	22.4	1	2.22E+06	4.50E-07
5	A-3958	15.5	1	1.18E+06	8.46E-07
6	T-130	1.42	1	3.84E+08	1.90E-06
		1.4	0.5	4.01E+08	
		6.92	0.5	3.32E+06	
		11.92	0.5	6.49E+05	
		10.78	0.5	8.78E+05	
		9.18	0.5	1.42E+06	
		4.8	0.5	9.95E+06	
7	T-130	6.2	1	9.23E+06	1.42E-07
		4.2	1	2.97E+07	
8	T-130	8.8	1	3.23E+06	3.57E-07
		4.7	1	2.12E+07	
9	A-6243	1.62	1	1.03E+09	4.95E-06
		27.92	1	2.02E+05	
10	A-6243	6.48	1	1.62E+07	6.35E-08
		1.7	1	8.96E+08	
		1.3	1	2.00E+09	

[a] See Figure 4-6 for location

[b] See Equation 3-2 in 3.3.1

4.3. *Goodman Diagram and Fatigue Life Evaluation*

Each bridge detail identified in Figure 4-6 was evaluated using the modified Goodman criterion. The development of the Goodman diagrams presented herein followed the calculations described earlier in 3.3.2. Construction documents indicate that the bridges considered are constructed of grade 50 steel with a yield stress of 50 ksi and ultimate strength of 65 ksi. The endurance limit, S_e, was calculated as 14 ksi using the Marin equation (see Appendix B). The resulting Goodman plots are shown in Figure 4-8, only showing the most critical fatigue detail in both the (a) skewed bridges and (b) non-skewed bridges.

Note that the Goodman diagrams consider the maximum in-plane principal stresses, as opposed to the maximum in plane stress component that was used in the damage calculation from the AASHTO detail categories; therefore, the stress ranges are greater than the values shown in Figure 4-6 and Table 4-2. Principal stresses are considered because crack growth is expected propagate in a direction perpendicular to the maximum in-plane stress. The five data points shown for each bridge represent the different load factors (1.5, 1.65, 1.75, 1.85, and 2.0) considered in the analysis.

In the skewed bridges, the critical fatigue details were identified as location 4 in bridge A-3958 and location 9 in bridge A-6243. In the non-skewed bridges, the critical fatigue details were identified as location 8 in bridge T-130 and location 1 in bridge A-3956. Figure 4-8 plots the stresses in each critical fatigue detail on the Goodman diagram for (a) the skewed bridges, and (b) the non-skewed bridges, for each of load factor. All of the data points within the skewed geometry fall within the finite fatigue life (unsafe) region of the Goodman plot; conversely, all of the data points within the non-skewed geometry are within the infinite fatigue life (safe) region, with the exception of the 2.0 load factor at location 1 in bridge A-3956. All of the other bridge details evaluated (locations 2, 3, 5, 6, 7, and 10) were within the infinite fatigue life region.

The data in Figure 4-8 clearly shows that skewed bridge construction is much more damaging to the steel component fatigue life than non-skewed construction. Partial depth web attachments found in the cross-frame or diaphragm to web connections within the skewed bridges were susceptible to higher stress ranges than in non-skewed bridges due to distortions in the girder web during the passage of the fatigue truck. Results from this analysis also show that an increase in the applied load (load factor) corresponds to a proportional increase in both the mean stress and stress amplitude. To shift the steel component life from finite fatigue life to infinite fatigue life, a localized retrofit utilizing pre-stressed CFRP is developed to reduce the mean stress to the safe region.

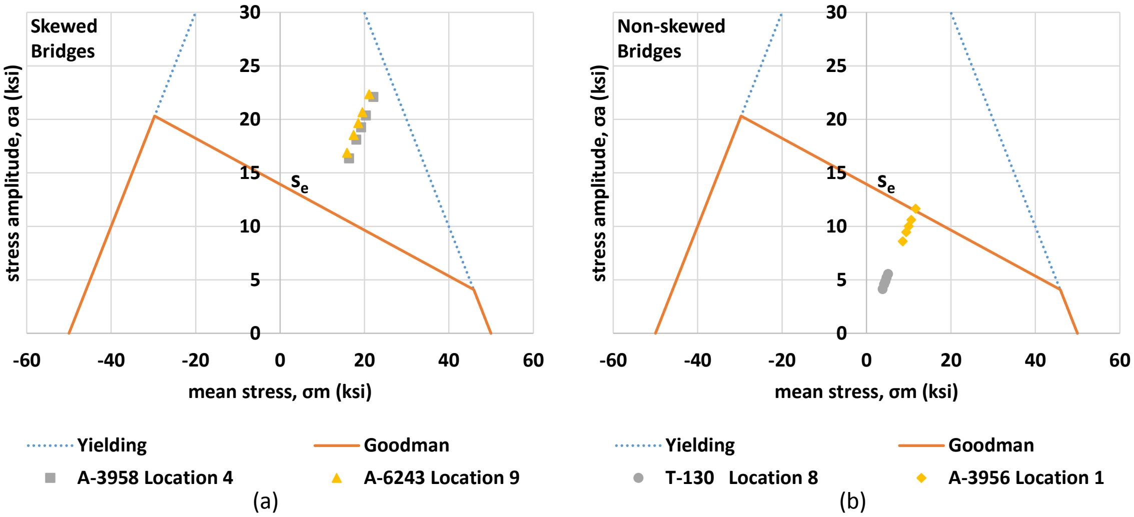

Figure 4-8: Goodman plots for the critical fatigue detail in the (a) skewed bridges (A-3958 & A-6243) and (b) non-skewed bridges (A-3956 & T-130)

5. Retrofits for Infinite Component Fatigue Life

5.1. *Development of Retrofit*

The retrofit developed in this work consists of stainless steel clamps and fixtures which can be locally installed near a structural detail. In this configuration, T-clamps are used to grip the CFRP material are inserted into a holder which is bonded to the structural component. The pre-stress is applied to the CFRP by separating the T-clamps from the holders using threaded bolts. Figure 5-1 shows the retrofit and illustrates the installation procedure. As shown in Figure 5-1, the CFRP is un-bonded from the structural member, while the holder is bonded to the structural member using structural adhesive. In this system, the CFRP material or parts of the metal fixtures can be easily replaced if necessary by simply loosening the bolts on the holders and T-clamps.

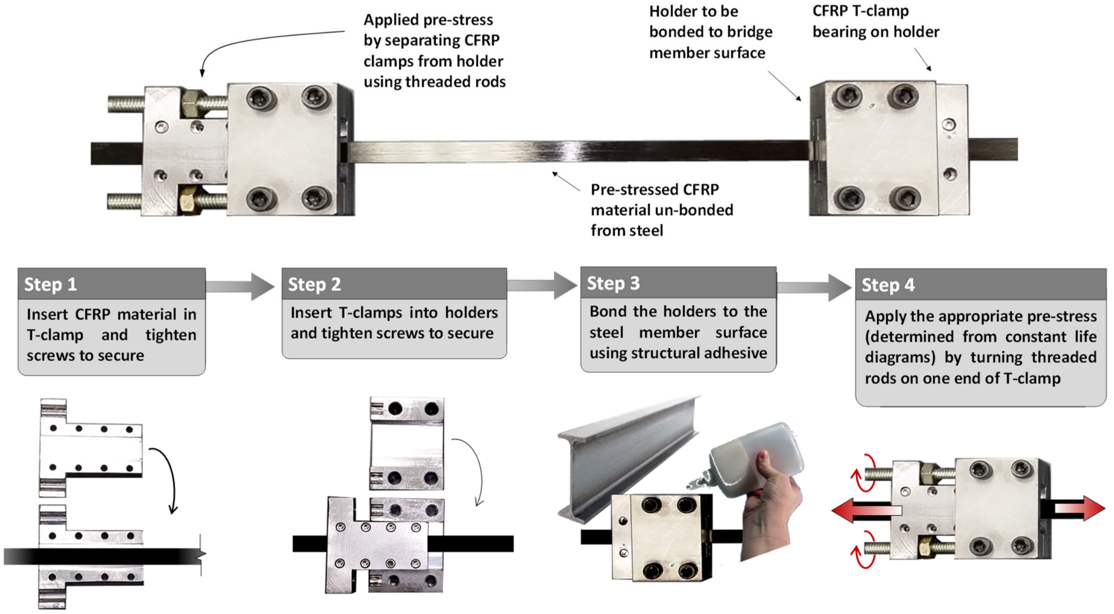
Applied pre-stress by separating CFRP clamps from holder using threaded rods

Holder to be bonded to bridge member surface

CFRP T-clamp bearing on holder

Pre-stressed CFRP material un-bonded from steel

Step 1 Insert CFRP material in T-clamp and tighten screws to secure

Step 2 Insert T-clamps into holders and tighten screws to secure

Step 3 Bond the holders to the steel member surface using structural adhesive

Step 4 Apply the appropriate pre-stress (determined from constant life diagrams) by turning threaded rods on one end of T-clamp

Figure 5-1: CFRP Retrofit and installation procedure

The retrofit can be installed locally at the critical fatigue region within common bridge connection details. Consider a partial depth web attachment similar to location 9 in Figure 4-6. Figure 5-2 shows how the pre-stressed CFRP retrofit may be installed to reduce the mean stress in this bridge detail. Crack growth is expected to occur at the weld toe between the transverse stiffener and the girder web. The retrofit should be installed perpendicular to the direction of crack growth so that the pre-stress force is acting to close the crack. The applied pre-stress will prevent crack initiation or crack propagation by shifting the mean stress in the structural detail to a safe limit on the Goodman diagram.

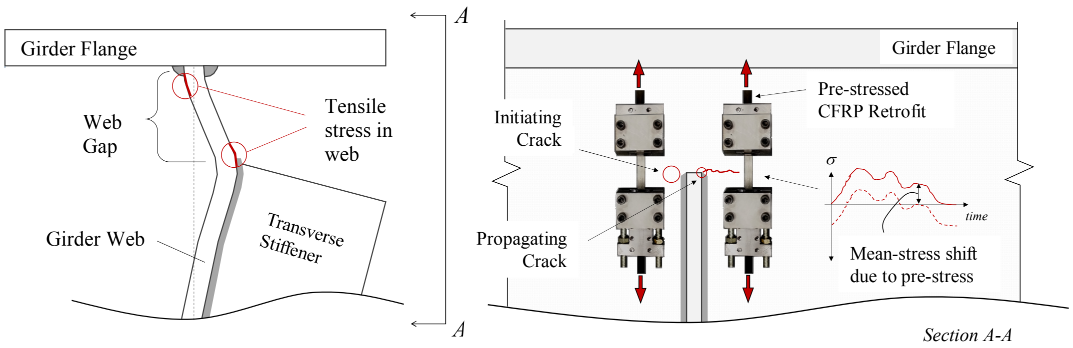

Figure 5-2: Example of retrofit installation on a partial depth web attachment showing shift in mean stress due to the pre-stressed CFRP.

5.2. *Development of Equations to Shift Component Life from Finite to Infinite Life*

The determination of the minimum pre-stress required to shift the component from a state of finite life to infinite fatigue life is based on the retrofit shown in Figure 5-1 and the Goodman constant life diagram. Let σ_{mi} and σ_{ai} represent the stresses in the structural detail before strengthening, corresponding to point A in the Goodman diagram shown in Figure 5-3. Point B, corresponding to the point (σ_{mf}, σ_{af}) represents the stress in the structural detail after installation of the retrofit. The shift in mean stress is indicated by $\Delta\sigma_m$ and is written as

$$\Delta\sigma_m = \sigma_{mi} - \sigma_{mf} \qquad \text{Equation 5-1}$$

where σ_{mf} is obtained by rewriting the Goodman equation in terms of mean stress shown in Equation 5-2. Due to the thin cross section and an elastic modulus similar to steel, the CFRP is assumed to add negligible stiffness to the component cross section; therefore, a negligible decrease in the stress amplitude is expected. As a result, σ_{ai} is equal to σ_{af} in the following equations.

$$\sigma_{mf} = \frac{S_{ut}}{n} - \frac{S_{ut}\sigma_{af}}{S_e} \qquad \text{Equation 5-2}$$

Substituting Equation 5-2 into Equation 5-1 gives

$$\Delta\sigma_m = \sigma_{mi} + \frac{S_{ut}\sigma_{af}}{S_e} - \frac{S_{ut}}{n} \qquad \text{Equation 5-3}$$

where $\Delta\sigma_m$ is the minimum compressive stress required to shift the mean stress from point A to point B, and n is a factor of safety.

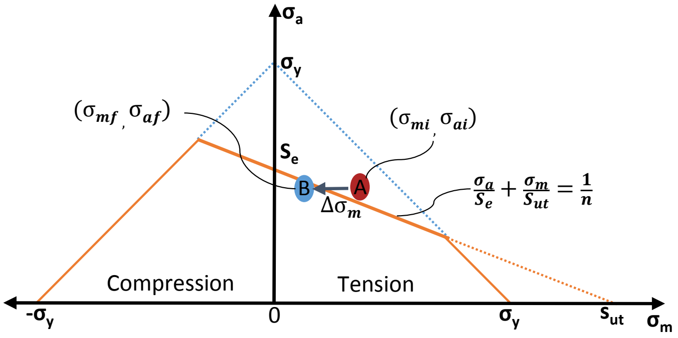

Figure 5-3: Shift in mean stress for infinite component life

The minimum pre-stress force (F_{pre}) corresponding to $\Delta\sigma_m$ can be determined through a cross section analysis of the structural component and retrofit configuration. Figure 5-4 shows the front and side view of the retrofit attached to a bridge girder web identifying the parameters needed to calculate F_{pre}. Considering the small area encompassed by the retrofit, $\Delta\sigma_m$ can be estimated as

$$\Delta\sigma_m = \frac{e\,F_{pre}\,t_w}{2\,I_m} + \frac{F_{pre}}{A_m} \qquad \text{Equation 5-4}$$

where t_w is the thickness of the girder web; A_m and I_m are the cross-sectional area and moment of inertia of a small region of the cross section encompassed by the retrofit; and e is the eccentricity between the CFRP material and the centroid of the girder web. Rearranging Equation 5-4 in terms of F_{pre} gives

$$F_{pre} = \frac{\Delta\sigma_m}{\frac{e\,t_w}{2\,I_m} + \frac{1}{A_m}} \qquad \text{Equation 5-5}$$

Finally, the minimum pre-stress required for infinite component fatigue life is written as

$$\sigma_{pre} = \frac{F_{pre}}{A_p} \qquad \text{Equation 5-6}$$

where A_p is the cross sectional area of the CFRP material.

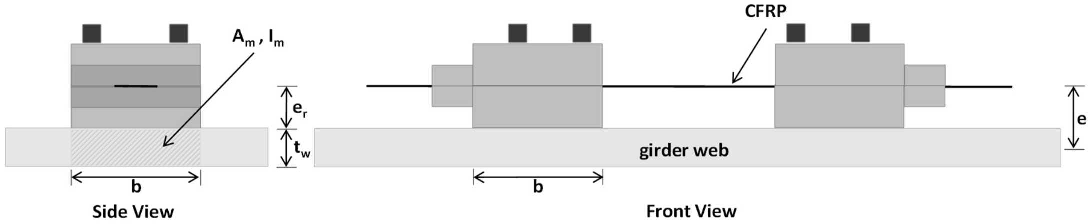

Figure 5-4: Front and side view showing dimensions of retrofit attached to a bridge component

5.3. *Minimum CFRP Pre-Stress Required for Infinite Component Fatigue life*

Table 5-1 shows the results of the calculations for $\Delta\sigma_m$ and F_{pre} following the procedure described above. Results are only shown for Location 4 in bridge A-3958 and Location 9 in bridge A-6243 (see 4.2, Figure 4-6) as these two details were the only components that contained stresses in the finite life region of the Goodman plot; all of the other bridge details evaluated (locations 2, 3, 5, 6, 7, and 10) were within the infinite fatigue life region. As discussed previously in this thesis, the bridges are constructed of grade 50 steel with a yield stress (S_y) of 50 ksi and ultimate strength (S_{ut}) of 65 ksi. The endurance limit (S_e) was predetermined as 14 ksi using the Marin equation (see Appendix B). The parameters necessary for the calculation of F_{pre} are shown in Figure 5-4 in which b=2.0 in. and e_r=0.5 in. Based on the construction documents, t_w=0.65 in. for bridge A-3958, and t_w=0.5 in. for bridge A-6243. The calculation was completed for the actual AASHTO fatigue I load factor (1.5) and four theoretical load factors (1.65, 1.75, 1.85, and 2.0). The data in Table 5-1 is plotted in Figure 5-5

Table 5-1: Calculation of pre-stress force (F_{pre}) required for infinite component fatigue life in critical details.

A-3958 Location 4					
AASHTO Fatigue I Load Factor	σ_{mi}	σ_{mf}	σ_{ai}, σ_{af}	$\Delta\sigma_m$	F_{pre}
1.5	16.35	-11.20	16.35	27.56	4.19
1.65	18.1	-19.36	18.1	37.46	5.69
1.75	19.25	-24.72	19.25	43.98	6.68
1.85	20.35	-29.85	20.35	50.20	Reduction in σ_a necessary
2	22.1	-38.01	22.1	60.11	Reduction in σ_a necessary
A-6243 Location 9					
AASHTO Fatigue I Load Factor	σ_{mi}	σ_{mf}	σ_{ai}, σ_{af}	$\Delta\sigma_m$	F_{pre}
1.5	15.92	-13.67	16.88	29.60	2.96
1.65	17.46	-21.41	18.54	38.88	3.89
1.75	18.56	-26.54	19.64	45.10	4.51
1.85	19.53	-31.34	20.67	50.87	Reduction in σ_a necessary
2	21.15	-39.17	22.35	60.32	Reduction in σ_a necessary

Figure 5-5(a) uses the Goodman plot to illustrate the minimum shift in mean stress ($\Delta\sigma_m$) and corresponding pre-stress force (F_{pre}) required for infinite component life, considering the AASHTO 1.5 fatigue I factor. According to Figure 5-5(a) and the data in Table 5-1, bridges A-3958 and A-6243 contain a similar mean stress and stress amplitude before strengthening, resulting in a similar shift in $\Delta\sigma_m$; however, F_{pre} varies due to differences between the two girder cross-sections. Bridge A-6243 has a smaller girder thickness (t_w), cross-sectional area (A_m) and moment of inertia (I_m), which reduces the F_{pre} required to reduce the mean stress.

Figure 5-5(b) plots the F_{pre} required for infinite life in the critical bridge details, considering AASHTO fatigue I load factors ranging from 1.5 to 2.0. According to Figure 5-5(b), the F_{pre} required for infinite life increases linearly as the load factor increases. F_{pre} increases more rapidly in bridge A-3958 than bridge A-6243. While the critical fatigue detail in these two bridges contain similar mean stresses and stress amplitudes, this plots shows that the a smaller web thickness in bridge A-6243 results in a slower rate of increase of F_{pre} as the load increases. As shown in Figure 5-5a), σ_a reaches its maximum at 20.3 ksi when σ_m is -29.7 ksi. The maximum value of σ_a is slightly exceeded for both bridge A-3958 and A-6243 when the factored load is 1.85 (refer to Table 5-1); therefore, a reduction in σ_a becomes necessary to achieve infinite fatigue life when the stress range corresponding to the 1.85 load factor is exceeded for these bridge details. As stated previously in this thesis, σ_a can be reduced by increasing the stiffness of the structural detail; however, if the increase in stiffness is achieved by enlarging the cross-section, F_{pre} will also increase.

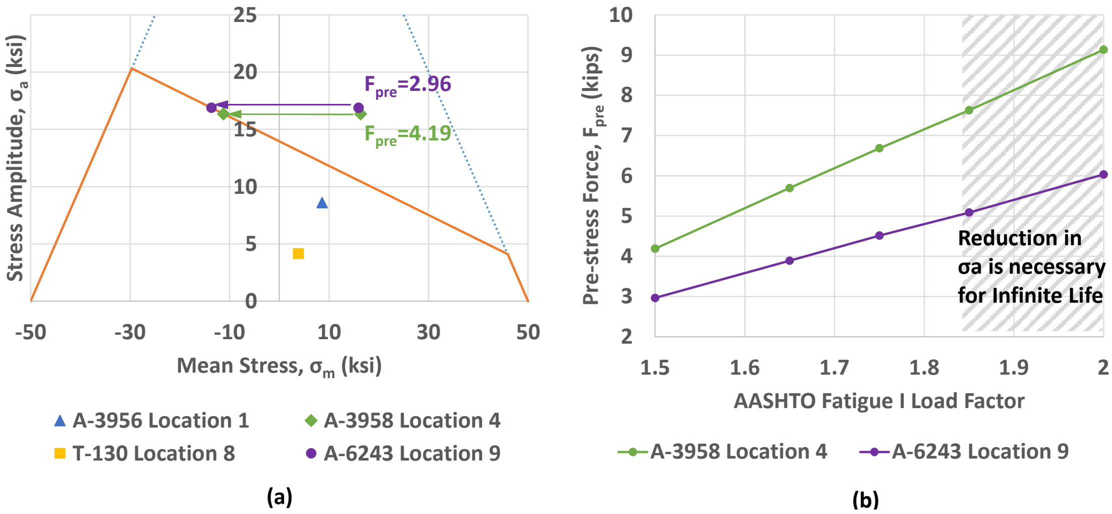

Figure 5-5: Minimum F_{pre} required for infinite fatigue component life in critical bridge details (a)illustrated in Goodman plot considering AASHTO 1.5 Fatigue I Load Factor (b) considering AASHTO Fatigue I Load Factors between 1.5 and 2.0

5.4. *Experimental Testing of Retrofit Solution*

A simple laboratory test was developed to evaluate the performance of the proposed pre-stressed CFRP retrofit system. In this experiment, a small-scale girder with a welded diaphragm connection is developed based on the cross frame configuration in bridge A-3958 (see 3.2.1, Figure 3-3). The beam is instrumented with strain gauges in order to compare readings before and after installation of the retrofit. Pictures of the experimental setup are shown in Figure 5-6. The diaphragm detail shown in Figure 5-6(c) is constructed of two L-shapes (1.5”×1.5”×0.125”) welded together to form a C-shape. The C-shape is welded to the face of a 1/8” steel plate, then welded to the web of a W8× section.

The beam is simply supported (see Figure 5-6(d)) and instrumented with two uniaxial strain gauges below the diaphragm detail on both sides of the beam. A third strain gauge is installed on the surface of the CFRP in order to measure the strain due to the applied pre-stress. Figure 5-6(b) shows the location of two of three the installed strain gauges. Strain gauges were installed on a smooth steel, achieved by cleaning and grinding the beam surface. A linear variable differential transformer (LVDT) (shown in Figure 5-6(a)) was used to measure local deflections of the beam during loading.

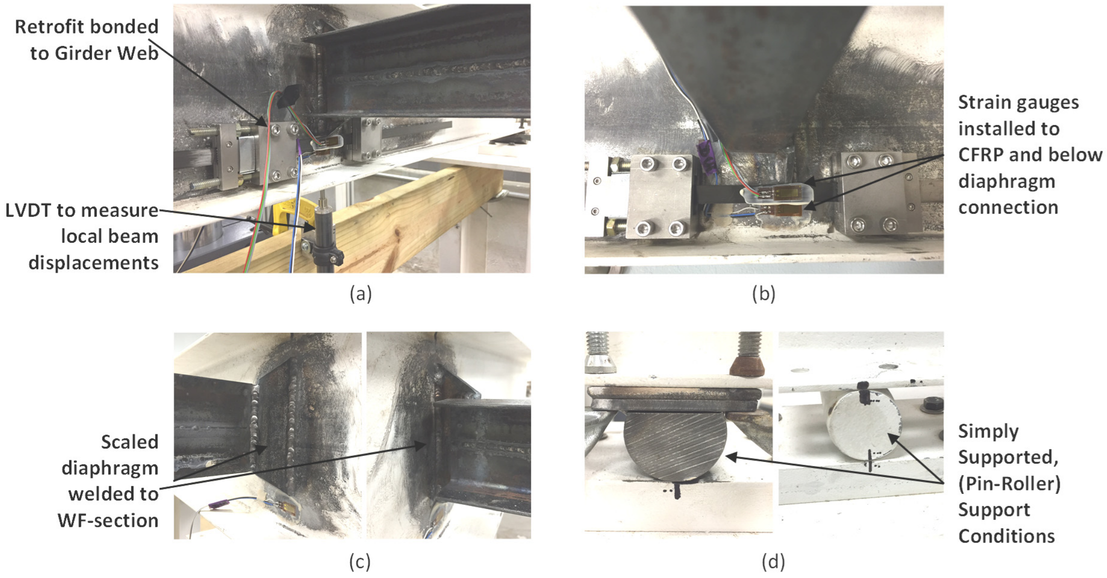

Figure 5-6: Pictures of experimental test setup showing (a) Retrofit bonded to structure, (b)installed strain gauges, (c) diaphragm to web connection detail, (d) test support conditions

The retrofit was bonded to the beam using structural adhesive as shown in Figure 5-5(a) and (b). The retrofit was installed over the strain gauge located below diaphragm connection in order to compare the strain readings beneath the diaphragm before and after pre-stressing the CFRP. Pre-stress was applied to the CFRP by hand turning the threaded bolts on the retrofit as described in 5.1. The beam was cyclically loaded in a three-point configuration, with the load applied at mid span above the diaphragm connection at a rate of 0.5 Hz.

Results of the experimental test show a shift in the stress range after the installation of the retrofit as shown in Figure 5-7. The stress was calculated using Hooke's law (σ=εE), assuming a typical steel young's modulus of 29,000 ksi. The mean stress under the applied load was 1.77 ksi before strengthening and 1.15 ksi after strengthening, resulting in a mean stress shift of 0.62 ksi.

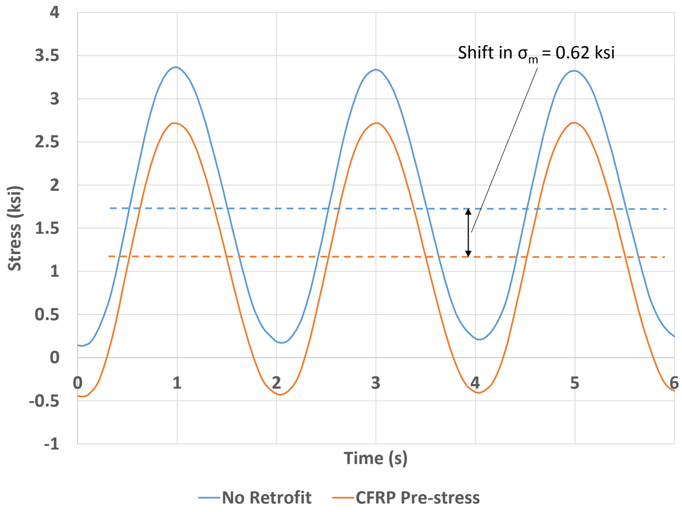

Figure 5-7: Shift in mean stress due to pre-stress under experimental testing

Although this experiment only provides a preliminary evaluation of the retrofit performance, the results indicate that the retrofit is capable of shifting the mean stress of structural details therein improving fatigue performance. One challenge faced during this experiment was preventing slip between the CFRP and the T-clamps. Attempts were made to increase the friction between the clamps and CFRP using heavy grit sand paper, but were unsuccessful as the pre-stress force increased. Bonding the CFRP to the T-clamps using structural adhesive may provide a more permanent solution suitable for a laboratory test at this scale. Ultimately, a thorough evaluation on slip and a new clamping configuration will need to be developed in further testing.

5.5. *Investigation into Bonding Strategies and Pre-Stress Loss*

In order for the CFRP retrofit to be effective, the bond between the retrofit components and existing steel sections must be capable of developing the CFRP pre-stress forces. Because the existing steel section surfaces may be corroded following years of exposure to harsh environments, quantifying bonding strengths between the retrofit and corroded steel surfaces is important. In addition to bonding strengths, pre-stress losses within the CFRP material, retrofit clamps, and bonding adhesives may affect retrofit performance over time. To investigate retrofit bonding strengths and pre-stress losses, experimental tests involving corroded steel plates, structural adhesives, prototypes of the developed retrofits, and local strain measurements were conducted. Figure 5-8 shows the initial test setup, where the retrofit is bonded to a corroded steel plate surface (representing a typical exposed steel girder surface) and instrumented with a uni-directional strain gauge for measurement of the initial applied pre-stress and resulting pre-stress losses. In the experimental setup shown in Figure 5-8, a two-part epoxy structural adhesives was used to bond the stainless steel retrofit component to the corroded steel plate.

During initial pre-stress, a corroded layer de-bonded from the steel plate, resulting in a complete loss of retrofit pre-stress. This de-bonding occurred at a CFRP pre-stress of near 70ksi; however, it is important to note that the adhesive did not fail. Review of the de-bonded clamp-holder surface indicated the removal of a corroded steel layer (see Figure 5-9). Figure 5-10(a) shows the pre-stress measurements for the retrofit-to-corroded-plate experiments.

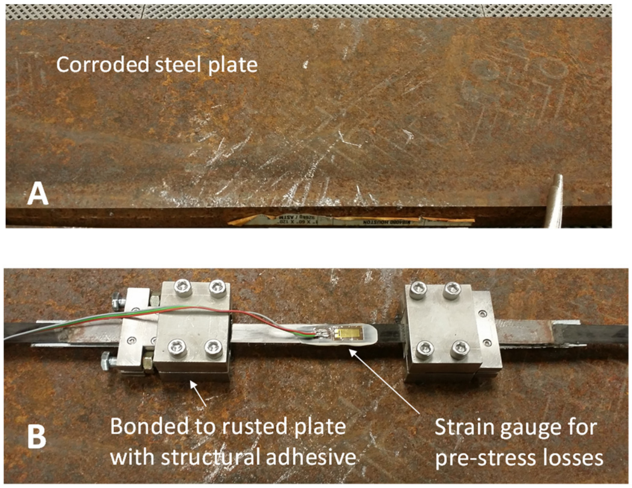

Figure 5-8: Corroded steel plate and bonded retrofit

Following the corrosion bond experiments, the steel plate surface was prepared by local grinding of the corroded layer, after which the retrofits were re-bonded using the two-part epoxy adhesive. Once the retrofit bond cured, a pre-stress of 56ksi was applied to the CFRP and measurements were taken every two hours to gauge pre-stress losses. Figure 5-10(b) shows initial pre-stress and gradual pre-stress loss within the CFRP over the entire 2,760 min measurement window. As shown in Figure 5-10(b), relaxation at the friction-clamp-to-CFRP interface led to a total loss of 5.83ksi over the initial two-day period, prior to the pre-stress stabilization. Alternative CFRP configurations, such as cylindrical CFRP rods with end chucks (similar to post-tension cable construction) may help reduce pre-stress losses.

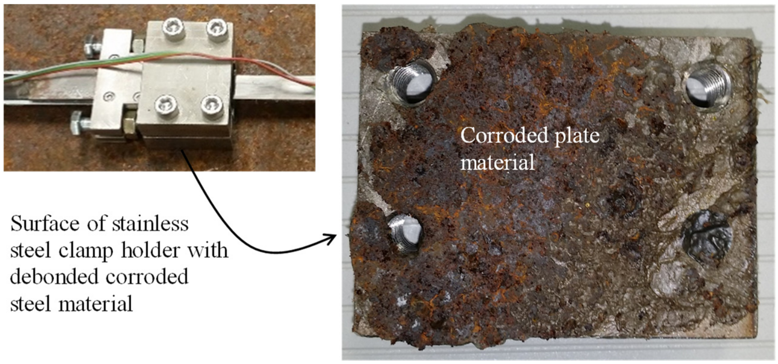

Figure 5-9: De-bonded retrofit with corroded plate material attached

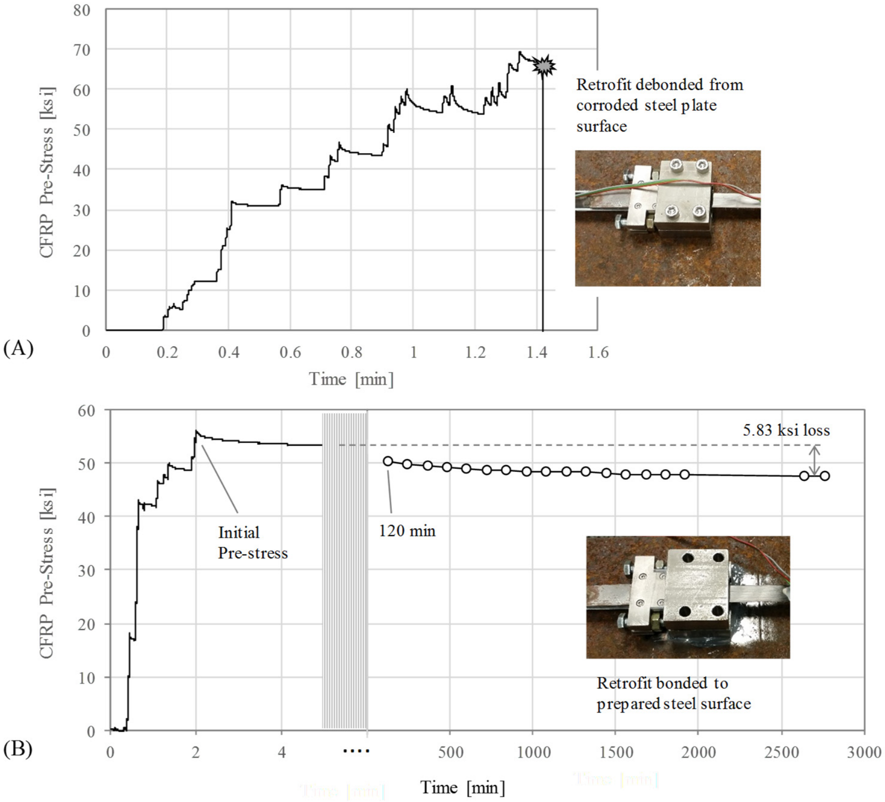

Figure 5-10: Prestress measurements for retrofits bonded to A) unprepared corroded steel surface, and B) prepared steel surface

6. Conclusions

6.1. *Summary of Main Findings*

A localized retrofit using pre-stressed CFRP material was developed to increase the fatigue capacity of common details within aged steel bridges. In this study, four stringer/multi-girder steel bridges with varying construction types were analyzed using finite element analysis. Critical fatigue details within each bridge are identified, and the fatigue performance is evaluated using the modified Goodman constant life diagrams. Finally, analytical formulations based on the Goodman diagrams are developed to determine the pre-stress force required to shift the stresses in critical details from a state of finite fatigue life to a state of infinite fatigue life. In addition to this analytical investigation, two experimental tests are conducted in which 1) a local bridge is instrumented with strain gauges and analyzed using finite element modeling; real-time strain measurements are compared with results of the finite element simulation during the passage of a truck along the bridge span, and 2) the function and performance of the developed retrofit is evaluated on a diaphragm to girder weld detail. The following conclusions were determined from the analytical and experimental results:

1. Finite element modeling using four-node linear shell elements provides a reasonable estimation of the actual strain measurements in an instrumented steel bridge. Results of the finite element analysis overestimated strain values by about 20-40 μin/in; however, the concrete bridge deck was excluded from the finite element model. Analytical results from the finite element analysis are conservative based on the modeling techniques used.

2. The Goodman fatigue evaluation showed that skewed bridge construction is more damaging to the steel cross-frame-to-girder component fatigue life than non-skewed construction. Cross-frame and diaphragm details within the skewed bridge geometry were susceptible to higher stress ranges during the passage of the fatigue truck due to distortion in the web of the longitudinal girder.

3. Using the Goodman criterion, the pre-stress force required to shift a structural detail from a state of finite fatigue life to infinite fatigue life increases linearly with the applied stress range; however, the magnitude of the pre-stressing force is dependent on the size of the steel member cross-section.

4. Laboratory tests were successful in shifting the mean stress in an instrumented steel beam using the localized retrofit having pre-stressed CFRP plates. Although this experiment only provides a preliminary evaluation of the retrofit performance, the results indicate that the retrofit is capable of reducing the mean stress of structural details therein improving fatigue performance.

5. Preparation of the steel surface (grinding away of corrosion) is needed prior to retrofit application, as the corroded surface layer is prone to de-bonding during retrofit pre-stress.

6. Retrofit pre-stress losses of near 10% within 48-hours could be expected for the configuration tested; however, alternative configurations using CFRP rods may help reduce these pre-stress losses.

References

American Association of State Highway and Transportation Officials (AASHTO). (1998). AASHTO LRFD Bridge Design Specifications. *AASHTO*, 2nd Edition.

American Association of State Highway and Transportation Officials (AASHTO). (2012). AASHTO LFRD Bridge Design Specifications. *AASHTO*, 6th Edition.

Dexter, R. J., & Ocel, J. M. (2013). Manual for Repair and Retrofit of Fatigue Cracking in Steel Bridges. *FHWA*, FHWA-IF-13-020.

Gangloff, R. P. (2005). Environmental Cracking— Corrosion Fatigue. In *Corrosion Tests and Standards.* ASTM- MNL20-2nd Edition-Chap. 26.

Ghafoori, E., Motavalli, M., Nussbaumer, A., Herwig, A., Prinz, G., & Fontana, M. (2015). Design criterion for fatigue strengthening of riveted beams in a 120-year-old railway metallic bridge using pre-stressed CFRP plates. *Elsevier*, Composites: Part B 68 1-13.

Huawen, Y., Konig, C., Ummenhofer, T., Shizhong, Q., & Plum, R. (2010). Fatigue Performance of Tension Steel Plates Strengthened with Prestressed CFRP Laminates. *ASCE Journal of Composites for Constuction*, Vol. 14. No. 5: 609-615.

Irvine, T. (2011, August 26). *Rainflow Cycle Counting in Fatigue Analysis.* Retrieved from http://citeseerx.ist.psu.edu/viewdoc/download?doi=10.1.1.444.3640&rep=rep1&type=pdf

Kaan, B., Alemdar, F., Bennett, C., Matamoros, A., Barrett-Gonzalez, R., & Rolfe, S. (2012). Fatigue Enhancement of Welded Details in Steel Bridges Using CFRP Overlay Elements. *ASCE Journal of Composites for Construction*, Vol. 16. No. 2: 138-149 .

Kopeliovich, D. (2012). *Carbon Fiber Reinforced Polymer Composites*. Retrieved from SubsTech Sustances & Technologies: http://www.substech.com/dokuwiki/doku.php?id=carbon_fiber_reinforced_polymer_composites

MacDonald, K. (2011). Fatigue design rules for welded structures. In *Fracture and fatigue of welded joints and structures.* Cambridge, UK: Woodhead Pub.

Marin, J. (1962). *Mechanical Behavior of Engineering Materials.* Englewood Cliffs, NJ: Prentice-Hall.

Mertz, D. (2012). Design for Fatigue. *Steel Bridge Design Handbook*, FHWA-IF-12-052-Vol. 12.

Miller, T. C., Chajes, M. J., Mertz, D. R., & Hastings, J. N. (2001). Strengthening of a Steel Bridge Girder using CFRP Plates. *Journal of Bridge Engineering*, Vol. 6-No. 6: 514-522.

National Association of Corrosion Engineers (NACE). (2012). *Highways and Bridges*. Retrieved from NACE International: https://www.nace.org/Corrosion-Central/Industries/Highways-and-Bridges/

Peiris, A., & Harik, I. (2015). Steel Bridge Girder Strengthening Using Postinstalled Shear Connectors and UHM CFRP Laminates. *ASCE. J.Perform. Constr. Facil.*, 29(5): 04014139. .

Schnerch, D., & Rizkalla, a. (2008). Flexural Strengthening of Steel Bridges with High Modulus CFRP Strips. *ASCE. Journal of Bridge Engineering*, Vol. 13, No. 2: 192-201.

Shigley, J., & Mischke, C. (1989). *Mechanical engineering design (5th ed,)*. New York: McGraw-Hill.

SIMULIA. (2012). *Abaqus/CAE User's Manual.* Providence, RI. : Dassault Systèmes Simulia Corp.

Svirsky, A. (2015). *National Bridge Inventory (NBI) Database.* Retrieved from NationalBridges: http://nationalbridges.com/

Teng, J. G., Chen, J. F., Smith, S. T., & Lam, L. (2002). FRP strengthened RC structures. (p. 245). Chichester, UK: John Wiley and Sons Ltd.

Appendix A. Rain-Flow Cycle Counting

Rain flow cycle counting is a technique used to count fatigue cycles in a stress history. Cycle counting techniques help to simplify complicated stress histories, allowing the application Miner's rule to assess the fatigue damage in a structural component. The rain flow method obtained its name from an analogy of rain dripping down a pagoda roof. The procedure for rain flow counting is described below.

Procedure for rain flow counting (Irvine, 2011):

1. Reduce the time history to a sequence of peaks and troughs.
2. Turn the sheet clockwise 90°, so the starting time is at the top
3. Imagine that the time history is a pagoda with water dripping down each peak and trough
4. Begin at the trough with the lowest value and count the number of half-cycles by looking for terminations in the flow occurring when either:
5. It reaches the end of the time history
6. It merges with a flow that started at an earlier trough; or
7. It encounters a trough of greater magnitude.
8. Repeat step 4 for each peak starting at the peak with the highest value.
9. Pair up half-cycles of identical magnitude (but opposite sense) to count the number of complete cycles.

This procedure is illustrated using the sample stress history shown in Figure A-1(a). Figure A-1(b) shows the labeled peaks and troughs and illustrated the "rain flow" in the stress history.

The total counts and the magnitude of each stress cycle is given in Table A-1, and the resulting cycle counts described in step 4 are as follows:

Counting Half Cycles:

Troughs: A-B, C-H, E-E', G-G'

Peaks: B-C, D-E, F-G, H-I

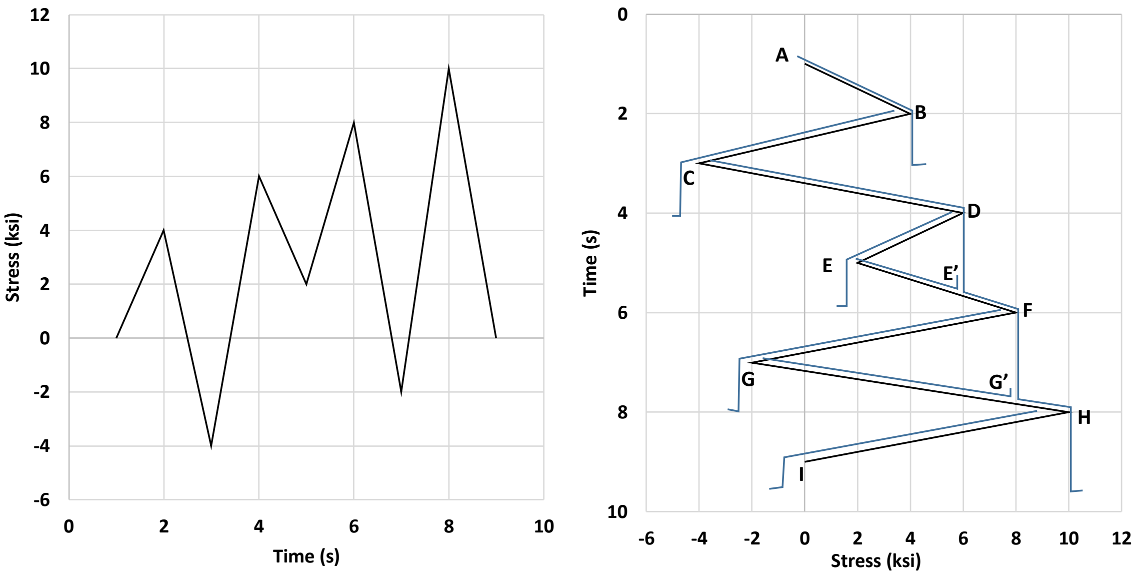

(a) (b)

Figure A-1: (a) Sample stress history (b) rain flow cycle counting procedure.

Table A-1: Total cycle counts, stress range, and path for sample stress history

Stress Range (ksi)	Number of Cycles, (n_i)	Path
4	0.5	A-B
14	0.5	C-H
8	0.5	B-C
10	0.5	H-I
4	1.0	D-E-E’
10	1.0	F-G-G’

Appendix B. Endurance Limit, S_e

This section describes the procedure for calculating the endurance limit, S_e, using the Marin equation. The process is described in detail in Shigley (1989). The Marin equation was given previously by Equation 3-7 and is shown here as Equation B-1.

$$S_e = k_a k_b k_c k_d k_e k_f S_e' \qquad \text{Equation B-1}$$

Se' is the endurance limit of the rotating beam specimen given previously by Equation 3-6 and is shown below as Equation B-2

$$S_e' = \begin{cases} .5\, S_{ut} & S_{ut} \le 200 ksi \\ 100\, ksi & S_{ut} > 200 ksi \end{cases} \qquad \text{Equation B-2}$$

B1. Surface factor k_a

The initiation of fatigue cracks often occurs at the free surface of the material. The surface modification factor is used to assess the quality of the finished surface and the tensile strength of the material. k_a is represented by Equation B-3, where a and b are the two coefficients given in Table B-1.

$$k_a = a S_{ut}^b \qquad \text{Equation B-3}$$

Table B-1: Parameters for Marin surface modification factor

Surface Finish	Factor a, S_{ut} given in ksi	Exponent b
Ground	1.43	-0.085
Machined or cold-drawn	2.70	-0.265
Hot-rolled	14.4	-0.718
As-forged	39.9	-0.995

B2. Size factor k_b

The size modification factor for rotation bar specimens were obtained through curve fitting of experimental results. This factor is based on the probability of failure for within a certain volume. As the volume increases, there is a higher probability of stress interaction with a critical flaw; therefore, the endurance limit decreases (Marin, 1962). For members that are subjected to bending and torsion, k_b is expressed as

$$k_b = \begin{cases} 0.879 d^{-0.107} & 0.11 \le d \le 2\ in \\ 0.91 d^{-0.157} & 2 < d \le 10\ in \end{cases} \qquad \text{Equation B-4}$$

For axial loading there is no size effect, therefore k_b=1. For members with non-circular cross-sections, an effective diameter d_e is used in place of d in Equation 8-4. For rectangular cross sections, d_e is given by

$$d_e = 0.808\sqrt{bh} \qquad \text{Equation B-5}$$

where b and h are the base and height of the cross-section, respectively. Equations to calculate de for other common structural shapes are given in Shigley (1989).

B3. Load factor k_c

The load modification factor considers whether axial, bending, or torsional loading is applied to a structure. Average values estimated for steel are given below.

$$k_c = \begin{cases} 1.0 & Bending \\ 0.85 & Axial \\ 0.59 & Torsion \end{cases}$$

B4. Temperature factor k_d

The ultimate strength (S_{ut}) varies under extreme temperatures. At high operating temperatures, the yield strength of steel is reduced and ductile failure is expected. At low operating temperatures, brittle fracture is expected in steel structures. Due to this reality, the endurance limit is similarly related to the tensile strength at extreme temperatures (Shigley, 1989). The following fourth order polynomial (obtained by curve fitting of experimental results) is used to calculate the temperature modification factor, where T_F is the temperature in degrees Fahrenheit for the range $70 \leq T_F \leq 1000$ °F.

$$k_d = 0.975 + 0.432(10^{-3})T_F - 0.115(10^{-5})T_F^{\,2} + 0.104(10^{-8})T_F^{\,3} - 0.595(10^{-12})T_F^{\,4} \quad \text{Equation B-6}$$

B5. Reliability factor k_e

Endurance strength data is often reported as average values. The reliability modification factor accounts for the scatter of experimental data. Reliability factors for some standard specified reliabilities assuming an eight percent standard deviation of the endurance limit are given in Table B-2

Table B-2: Reliability factors corresponding to 8% standard deviation of the endurance limit

Reliability, %	Reliability Factor k_e
50	1.000
90	0.897
95	0.868
99	0.814
99.9	0.753
99.99	0.702
99.999	0.659
99.9999	0.620

B6. Miscellaneous-Effects Factor k_f

The miscellaneous-effects modification factor accounts for other various effects that the material may be subjected to during service. This factor may consider corrosion, electrolytic plating, metal spraying, cyclic frequency, and frottage corrosion (Shigley, 1989). These values are not easily attained; therefore, the miscellaneous-effects factor is assumed to be 1.0 in this work.

B7. Calculation of S_e

The endurance limit, S_e, was calculated for each bridge. Results of this calculation are described here for bridge A-6243. Reasonable assumptions were made for calculations of the modification factors due to limited information about the bridge steel. Using Equation B-3 and assuming a hot rolled finish assumption, the surface modification factor was calculated as k_a=0.719. The critical fatigue region in bride A-6243 was located at the weld between the cross-frame and the girder web; therefore the size factor was calculated considering cross-section of the girder web (0.5in x 48 in). Using Equation B-5 the effective diameter of the web was calculated as d_e=3.958 in. Substituting this value into Equation B-4 results in a size factor of k_b=0.733. Assuming a combination of bending and axial loading, the load factor was approximated as k_c=0.95. Using Equation B-6 and assuming a normal operating temperature of 70°F, the temperature factor was calculated as k_d=1.0. A reliability factor of 95% is considered for the analysis, which results in k_e=0.868. The bridges were constructed using Grade 50 steel with an ultimate strength (S_{ut}) of 65 ksi. Using Equation B-2 endurance limit of the rotating beam specimen was calculated as S_e'=32.5 ksi. Substituting these values into the Marin equation (Equation B-1), results in an endurance limit of S_e=14 ksi. A similar value was calculated for each of the four brides, therefore an endurance limit of S_e=14 ksi is used for all Goodman analyses.

[Page Intentionally Left Blank]